Monthly Notices
of the
ROYAL ASTRONOMICAL SOCIETY

MNRAS **440,** 365–386 (2014)
Advance Access publication 2014 March 10

doi:10.1093/mnras/stu170

Identification of 23 accreting binaries in the Galactic Bulge Survey

M. A. P. Torres,[1⋆] P. G. Jonker,[1,2,3] C. T. Britt,[4,5] C. B. Johnson,[4] R. I. Hynes,[4] S. Greiss,[6] D. Steeghs,[6] T. J. Maccarone,[5] F. Özel,[7] C. Bassa[8] and G. Nelemans[3,9]

[1]*SRON, Netherlands Institute for Space Research, Sorbonnelaan 2, NL-3584 CA Utrecht, the Netherlands*
[2]*Harvard–Smithsonian Center for Astrophysics, 60 Garden Street, Cambridge, MA 02138, USA*
[3]*Department of Astrophysics IMAPP, Radboud University Nijmegen, Heyendaalseweg 135, NL-6525 AJ Nijmegen, the Netherlands*
[4]*Department of Physics and Astronomy, Louisiana State University, Baton Rouge, LA 70803-4001, USA*
[5]*Department of Physics, Texas Tech University, Box 41051, Lubbock, TX 79409-1051, USA*
[6]*Department of Physics, University of Warwick, Coventry CV4 7AL, UK*
[7]*Department of Astronomy, University of Arizona, 933 N. Cherry Ave., Tucson, AZ 85721, USA*
[8]*Jodrell Bank Centre for Astrophysics, The University of Manchester, Manchester M13 9PL, UK*
[9]*Institute for Astronomy, KU Leuven, Celestijnenlaan 200D, B-3001 Leuven, Belgium*

Accepted 2014 January 20. Received 2014 January 20; in original form 2013 October 2

ABSTRACT

We present the identification of optical counterparts to 23 GBS X-ray sources. All sources are classified as accreting binaries according to the emission-line characteristics inferred from medium-resolution spectroscopy. To distinguish accreting binaries from chromospherically active objects, we develop criteria based on Hα and He I $\lambda\lambda$5786, 6678 emission-line properties available in the literature. The spectroscopic properties and photometric variability of each object is discussed and a classification is given where possible. At least 12 of the 23 systems show an accretion-dominated optical spectrum and another 6 show stellar absorption features in addition to emission lines indicating that they are probably accreting binaries in quiescence or in a low accretion rate state. Two sources are confirmed to be eclipsing: CX207 and CX794. CX207 is likely a magnetic cataclysmic variable (CV), while CX794 is a nova-like CV in the period gap. Finally, the large broadening (2100 km s^{-1} FWHM) of the Hα emission lines in CX446 and CX1004 suggests that they are also high-inclination or even eclipsing systems. Whether the compact object is a white dwarf in an eclipsing CV, a neutron star or a black hole in a high-inclination low-mass X-ray binary remains to be established.

Key words: accretion, accretion discs – black hole physics – techniques: radial velocities – binaries: close – stars: neutron – X-rays: binaries.

1 INTRODUCTION

We are undertaking a multiwavelength survey to characterize the X-ray sources found with the *Chandra* X-ray observatory in a strip of fields in a pair of $6^\circ \times 1^\circ$ areas centred $1\overset{\circ}{.}5$ above and below the Galactic plane. This so-called Galactic Bulge Survey (GBS) targets X-ray emitting binaries in the direction towards and in the Milky Way bulge with the primary goals of finding quiescent low-mass X-ray binaries (qLMXBs) and derive the number ratio of LMXBs and cataclysmic variables (CVs) in this sample in order to determine constraints on the binary evolution, in particular the common envelope phase. The GBS is designed to search for both X-ray sources and their optical counterparts. The regions covered by the GBS area are chosen to avoid the high optical extinction and crowding found in the mid-plane. The full survey area has been observed in X-rays with the *Chandra* X-ray observatory to a 0.5–10 keV flux limit of $(1-3) \times 10^{-14}$ erg cm^{-2} s^{-1}. The GBS area has been also imaged in optical bands with the CTIO 4-m Blanco telescope to typical upper limits of r', $i' \lesssim 23$.

A total of 1640 unique X-ray sources have been found (Jonker et al. 2011, 2014), providing a large sample to fulfil the two main goals of this project. In what follows, we briefly describe these goals, while the specific details concerning the GBS can be found in Jonker et al. (2011, 2014). The first GBS goal involves quantifying dynamically the masses of compact objects in eclipsing qLMXBs in order to constrain the neutron star equation of state and black hole formation models. This requires us to identify new X-ray binaries with optical counterparts suitable for dynamical studies. These studies will allow one to measure the masses of compact objects,

⋆ E-mail: M.Torres@sron.nl

with unprecedented accuracy in the case of eclipsing systems. To facilitate achieving this objective, the limiting sensitivity for the X-ray imaging was selected to maximize the number of detected qLMXBs with respect to new CVs. The expectation is to detect in X-rays more than 200 qLMXBs with 120 of them having detectable counterparts in the GBS optical images. In comparison, the current number of known LMXBs in the Galaxy exceeds 170 (see e.g. Özel et al. 2010). More than half of them are persistently X-ray bright, making them usually unsuitable for dynamical studies due to the lack of spectral features from the donor star in their optical spectra. In contrast, the photosphere from the donor star is expected to contribute significantly to the optical spectra of qLMXBs. Nowadays, the census of LMXBs grows each year by a few with the discovery of transient LMXBs during unpredictable X-ray outbursts. Once in quiescence, optical counterparts are detected for sources not affected by severe reddening and/or crowding issues. The GBS instead represents a systematic effort to identify a large sample of new qLMXBs with optical counterparts suitable for further follow-up. A sample consisting of systems that have not undergone a recent outburst will allow us to establish if there exist selection effects that arise from the current sample of persistent objects and transients that have suffered outbursts in the past few decades.

The second GBS objective is to investigate binary formation and evolution scenarios, including the study of kicks during the supernova event that produces the compact primary in an LMXB. The method employed to achieve this goal involves comparing the observed number of sources per source class with the number of sources predicted by binary population synthesis calculations. The calculations presented in Jonker et al. (2011) predicted a total of 1648 X-ray sources in the GBS area with more than half expected to be CVs and chromospherically active binaries while a minor fraction (tenths or below) are to be persistent LMXBs, Be X-ray binaries and ultracompact X-ray binaries. The predicted total number of GBS sources is in very good agreement with the 1640 sources detected in X-rays. To allow detailed comparisons, multiwavelength and variability studies are in progress to identify and characterize counterparts to the GBS sources. See e.g. Udalski et al. (2012) and Hynes et al. (2012a) for a photometric search and study of GBS sources with bright or moderately bright optical counterparts, Greiss et al. (2014) for the identification of counterparts at infrared bands, Britt et al. (2013) for the optical spectroscopic identification of five accreting binaries, Maccarone et al. (2012a) for the characterization of GBS sources with bright radio counterparts, Ratti et al. (2013a) for the first dynamical study of a GBS source and Hynes et al. (2014) for the identification of a symbiotic X-ray binary. The GBS and related data are also being used to study recently discovered X-ray transients or previously known (but poorly studied) sources showing renewed activity (e.g. Greiss et al. 2011a,b; Hynes et al. 2012b; Maccarone et al. 2012b; Rojas et al. 2012).

In order to identify the optical counterparts, we are acquiring spectra for the candidate counterparts found within the error circle for the accurate *Chandra* X-ray position. Large-aperture telescopes are being used to target qLMXBs which are expected to be faint as they suffer from reddenening and are located at kiloparsec distances. For instance, the unreddened apparent magnitude and colours of a (donor) star at a distance of 8 kpc are $(r', r'-i', r'-K)_0 = (17.4, 0.1, 0.9)_0$ for F0 dwarfs and $(23.6, 1.3, 3.4)_0$ for M2 dwarfs. Taking into account reddening, the predicted apparent magnitudes for active LMXBs in the GBS area is $18 < i' < 21$, while qLMXBs are expected to have $i' > 20$ (Jonker et al. 2011).

In this paper, we focus on 23 GBS objects that we have selected as new accreting binaries on the basis of Hα and He I $\lambda\lambda$5786, 6678 emission-line properties. The identifications are results obtained from spectroscopy with the Very Large Telescope and Magellan telescopes of optical counterpart candidates to GBS X-ray sources. Candidate counterparts were selected for follow-up spectroscopy on the basis of positional coincidence of optical sources with the X-ray source, variability and/or colours (see e.g. Greiss et al. 2014; Britt et al., in preparation).

We begin by describing in Section 2 the spectroscopic and photometric observations. In Section 3, we explain how the data were processed. In Section 4, we present and discuss the results for the 23 sources. Accurate coordinates, finding charts, optical light curves from the Blanco 4-m telescope and spectra of medium resolution (∼5, 10 Å) and relatively large wavelength coverage are provided for each object. Finally, in Section 5, we consider how to overcome the selection bias towards emission-line objects that single epoch spectroscopic surveys will suffer from. In this paper, we will follow the designation to the sources introduced in Jonker et al. (2011): CX *N* where *N* is the source number in the count-rate-sorted GBS catalogue.

2 OBSERVATIONS AND DATA REDUCTION

2.1 VIMOS (VIsible Multi-Object Spectrograph)

VIMOS (Le Fèvre et al. 2003) is a 4-channel imager and multi-object spectrograph mounted on the Nasmyth focus of the 8.2-m ESO Unit 3 Very Large Telescope at Paranal, Chile. Each channel (a.k.a. quadrant) covers a field of view of about 7×8 arcmin^2. The four quadrants are separated by approximately 2 arcmin wide gaps. The current VIMOS detectors are 2048×4096 pixel EEV CCDs that provide a 0.205 arcsec pixel^{-1} scale. Prior to 2011 August VIMOS was equipped with EEV CCDs of same format as the new detector, but with both lower sensitivity and strong fringing in the red. The GBS sources CX73 and CX772 were observed using the old CCDs.

During the observations VIMOS was operated in multi-object spectroscopy (MOS) mode. In this mode laser-cut slit masks are inserted at the entrance focal plane permitting spectroscopy of optical counterpart candidates to several GBS sources in a single exposure. The slit masks are prepared using the VIMOS Mask Preparation Software (VMMPS) tool (see Bottini et al. 2005). VMMPS uses pre-images of the fields as reference frames to define the slit and secure objects well-centred at the slit positions after telescope acquisition of the field. All slits were designed with a 1.0 arcsec width. Their length and location were determined per GBS source to include more than one optical counterpart candidates if possible, to secure areas for sky subtraction during the data reduction and/or to avoid strong saturation of bright sources. Thus, the identified counterparts were not necessarily centred on their slits.

We selected the medium-resolution grism that yields a 2.5 Å pixel^{-1} dispersion and a wavelength coverage of ∼4800–10 000 Å. The exact coverage depends on the location of the small slit with respect to the CCD boundaries as some part of the dispersed spectrum may fall off the chip. The GG475 order-sorting filter was used to avoid overlap between the first and second grating orders when observing bright sources. The use of 1.0 arcsec width slits provided a spectral resolution of about 10 Å full width at half-maximum (FWHM) corresponding to 460 km s^{-1} at Hα and 350 km s^{-1} at 8600 Å.

The spectroscopic observations were obtained in service mode under programmes 085.D–0441(A) and 087.D-0596(A). One hour observing blocks (OBs) were executed per pointing, consisting

Table 1. Source position (J2000) and log of the VIMOS and Mosaic-II observations.

No.	GBS ID	α (deg)	δ (deg)	VIMOS OB ID (spectroscopy)	VIMOS OB ID (pre-imaging)	VIMOS Quadrant	Date UT (spectroscopy)	Mosaic-II *N* frames
1	CX28	264.945 77	−27.302 454	453466	509361	4	2011-04-02	28
2	CX39	265.416 81	−27.293 867	508808	453460	1	30-03-2011	29
3	CX44	268.928 44	−28.302 561	–	–	–		19
4	CX45	263.910 52	−28.881 077	575808	453494	1	04-07-2011	26
5	CX63	263.547 55	−29.521 61	575585	453506	2	30-06-2011	35
6	CX64	264.511 63	−28.524 092	575148	453474	3	09-06-2011	18
7	CX70	263.896 18	−29.994 881	577698	453498	1	01-07-2011	35
8	CX73	266.197 97	−27.017 094	484756	453436	2	09-05-2010	27
9	CX87	264.200 65	−29.610 935	575612	453490	2	03-07-2011	21
10	CX93	266.186 65	−26.058 428	509202	453434	2	29-04-2011	35
11	CX128	265.118 25	−27.193 412	509361	453466	2	02-04-2011	18
12	CX137	268.971 95	−28.276 145	577805	544378	1	22-07-2011	4
13	CX142	266.015 67	−31.384 749	577743	544353	4	26-06-2011	16
14	CX154	264.661 28	−28.594 275	575008	453472	3	26-05-2011	26
				575148	453474	2	09-06-2011	–
15	CX207	266.606 28	−26.526 409	508997	453430	2	02-05-2011	35
				575272	453430	2	06-06-2011	–
16	CX377	265.818 91	−27.760 318	575026	453452	1	28-05-2011	35
				575799	453452	1	23-07-2011	–
17	CX446	266.613 21	−25.831 265	508787	453428	1	02-05-2011	37
18	CX522	268.635 42	−28.488 336	575918	544379	4	04-08-2011	–
19	CX772	266.021 07	−26.533 16	484978	453440	2	11-05-2010	30
20	CX781	265.796 43	−27.272 709	575403	453446	2	27-07-2011	38
21	CX794	265.426 55	−27.975 036	509817	453456	1	03-04-2011	28
				575275	453456	1	26-05-0211	–
22	CX1004	266.597 81	−31.097 159	577836	544354	2	28-06-2011	35
23	CX1011	266.519 62	−31.289 573	577836	544354	4	28-06-2011	28

of acquisition imaging, two spectroscopic integrations of 875 s, three flat-field exposures and a helium–argon lamp exposure for wavelength calibration. The standard data reduction steps were performed with the ESO-VIMOS pipeline (Izzo et al. 2004). These include bias subtraction, bad-pixel correction, wavelength calibration and removal of the instrumental response. The typical root mean square (rms) for the wavelength calibration fit was <0.1 pixels. The pipeline averages the two spectra and extracts automatically the objects found in each slit.

The pipeline data products were examined to identify any problems with the extraction of the spectra. This examination showed that the output spectra for isolated objects were satisfactory in terms of extraction quality. This was not the case for partially resolved sources where the choice of the aperture size for the object, sky subtraction regions and tracing become critical steps during the extraction process. Thus, we extracted interactively with the IRAF KPNOSLIT package all reduced 2D frames that contain both stellar and sky spectra (pipeline files with product code SSEM). For partially resolved sources in crowded fields, the object and sky apertures were sized to maximize the number of pixels contributing to the object and sky, respectively, and to minimize the contribution from any field star/s. Checks for the stability of the wavelength calibration were made for each object looking at the strongest atmospheric emission lines present in the spectra. We made use of the [O I] λ6300.3 line and/or the OH emission at λλ6863.96, 9872.14 Å (Osterbrock et al. 1996; Osterbrock, Fulbright & Bida 1997). In this way, we estimate that the median amplitude of the radial velocity (RV) error is $\lesssim$20 km s^{-1}. Zero-point corrections were applied only to the spectra of the sources CX70 and CX377 which showed RV offsets in the [O I] and OH emission lines' wavelengths well above the distribution of the internal RV error.

In a few cases, the observing conditions were not good during the OB execution and the OB was repeated later under the weather conditions requested for the programme. Spectra of an optical counterpart extracted from different OBs were combined if they were acquired close in time and if there were no significant changes in the spectra between observations. A log of the VIMOS observations is presented in Table 1 in which identification numbers for the GBS sources, pre-imaging OBs and spectroscopic OBs are given. The observing date and the quadrant where the object was detected are also provided.

2.2 IMACS (Inamori-Magellan Areal Camera and Spectrograph)

The GBS sources CX44 and CX1011 were observed with IMACS (Bigelow & Dressler 2003) which is mounted on the 6.5-m Baade-Magellan telescope at Las Campanas Observatory. Both objects were observed on the night of 2011 May 15 UT with IMACS operated in short-camera mode. In this mode, the spectra are dispersed along the long axis of two of the eight 2112 × 4160 pixel E2V CCDs with 0.20 arcsec pixel^{-1} scale. We used a 300 line mm^{-1} grism centred at 6700 Å yielding a dispersion of 1.15 Å pixel^{-1} (CCD no. 3) and 1.31 Å pixel^{-1} (CCD no. 8) in the spectral intervals 3450–6660 and 6750–10 410 Å, respectively. Together with a 1.0 arcsec wide slit, the instrumental setup achieved a spectral resolution of ∼5 Å FWHM corresponding to 230 km s^{-1} at Hα and 175 km s^{-1} at 8600 Å. A single spectrum was acquired per source with an integration time of 1200 and 900 s for CX44 and CX1011, respectively. The flux standards Feige 56, Feige 57 and LTT 3864 were also observed in order to correct for the instrumental response.

The IMACS frames were bias and flat-field corrected with standard IRAF routines. The spectra were extracted from each CCD frame with the IRAF KPNOSLIT package. The pixel-to-wavelength calibration was derived from cubic spline fits to HeNeAr arc lines. The rms deviation of the fit was $\lesssim$0.06 Å. The sky [O I] λ6300.3 line and the OH emission blend at 7316.3 Å show that the accuracy of the wavelength calibration of the spectra from both CCDs is $\lesssim$0.08 Å.

2.3 NOAO Mosaic-II imager

We acquired time-resolved photometry from 2010 July 12–18 with the Mosaic-II instrument mounted on the Blanco 4-m telescope at the Cerro Tololo Inter-American Observatory. Multiple 120 s exposures of 45 overlapping fields were taken to cover a 9 deg^2 area in the Sloan r'-band containing the GBS X-ray sources reported in Jonker et al. (2011). The order in which the fields were visited was randomized to minimize aliasing caused by regular sampling. Typical seeing conditions during the observations were around 1 arcsec. The last column of Table 1 provides the number of frames containing a detection of the optical counterpart to a GBS source. No photometric data are available for CX522 as the source is unresolved from a bright field star in the Mosaic-II data.

The data were reduced via the NOAO Mosaic Pipeline which searches and corrects for instrumental artefacts in the image such as cross talk between CCDs. The pipeline applies bias and flat-field corrections, and adds a world coordinate system for each image based on USNO-B1 stars in the field. An estimate of the photometric zero-point of the images is also made by comparing the instrumental magnitude of the field star to their USNO B1.0 apparent magnitudes. A detailed explanation of the data reduction procedures can be found in chapter 2 of the NOAO Data Handbook (Shaw 2009).

3 DATA ANALYSIS

3.1 Spectroscopy

Given the uncertain reddening towards the GBS sources and thereby uncertain intrinsic colours, the classification of optical counterparts in this paper was based on the identification of spectral lines and not on the optical continuum measurements. Thus, the reduced spectra were normalized by fitting cubic splines to the continuum after masking emission lines, telluric bands and instrumental artefacts. Relevant spectral features were identified and studied. These include late-, early- or white dwarf-type photospheric lines, emission lines and diffuse interstellar bands (DIBs). The normalized spectra of the accreting binaries discussed in this paper are presented in Figs 1–3. For the sake of identification, the rest wavelengths for the following lines are marked in all figures: Hβ, He I λ5876, Hα and He I λλ6678, 7065 (left-hand panels). In the right-hand panels, the markers correspond to the Na I doublet λλ8183, 8195, Ca II λ8498, P16, Ca II λ8542, P15, P14, Ca II λ8662, and P13/12/11/10/9 and 8 (here, Pn stands for the Paschen $n-3$ transition).

Strong features were examined manually with the *splot* task in IRAF obtaining their RV, FWHM and equivalent width (EW). The two first parameters were measured by fitting the line profiles with a Gaussian function, whereas the EW was measured by means of the *splot* keystroke *e*. Table 2 reports the values for the strongest emission lines except for lines which do not have a well-defined profile due to noise and/or telluric contamination problems. Their uncertainties were estimated by looking at the scatter in the values when selecting different wavelength intervals to set the local continuum level. Finally, note that all radial velocities provided in the work are heliocentric ones. The EW values are positive in order to allow in the next sections for an easy comparison with previous studies where the emission line EWs are given as positive.

3.2 Astrometry

Coordinates for the optical counterparts to the 23 GBS sources discussed in this work are provided in Table 1. Except for CX44, they were obtained from the VIMOS pre-images after performing an astrometric calibration that delivered a position accurate to $\lesssim$0.2 arcsec. The astrometric solution was calculated against entries from the third US Naval Observatory CCD Astrograph Catalogue (UCAC3; Zacharias et al. 2010). Between 90 and 900 UCAC3 objects were found in the pre-images. We fitted for the reference point position, the scale, the position angle and image distortion. The rms of the fits was typically $\lesssim$0.1 arcsec. The position for the optical counterpart to CX44 was derived from Mosaic-II images (see Section 2.3). Finding charts 20 arcsec × 20 arcsec wide are shown on-line in Appendix . Observers requiring wider charts can find in Table 1 the necessary details to retrieve from the ESO archive the pre-images for the target of interest.

3.3 Photometry

Photometry was performed on the Mosaic-II r'-band data (Section 2.3) using the image subtraction package ISIS (Alard & Lupton 1998; Alard 2000). ISIS uses a reference image which is convolved with a kernel in an effort to match a subsequent image of the same field. This subsequent image is then subtracted from the convolved reference image. Stars which do not vary in magnitude should subtract cleanly, such that the subtracted image is clear of non-variable objects. Therefore, any residual flux is due to an inherent change in brightness of a source. ISIS performs point spread function (PSF) photometry on the subtracted images. The model of the PSF used in each image is build by convolving the PSF model in the reference image with the kernel solution.

In order to save computation time, 104 arcsec × 104 arcsec cutouts of the full Mosaic-II images around the position of each X-ray source were taken for processing. The resulting ISIS images were examined by eye to identify variable objects near or at the X-ray positions of the GBS sources. Light curves were then built for these variables and Lomb–Scargle periodograms were used to search for periodicities if enough data points were available. Ellipsoidal modulation is expected in close binaries, in particular in accreting binaries in which the donor star dominates the light curve. We took into account that this type of photometric variability has two maxima and minima in a single orbital cycle and checked periods twice as long as prominent peaks on a periodogram. We also consider both aliases and harmonics, as higher harmonics can sometimes appear at a higher power than the fundamental frequency. In Fig. 4 we show a sample of light curves characterized by outburst brightenings events, periodic modulation or long-term variability. In Appendix A, the reader will find the remaining light curves which are in most cases consistent with flickering variability.

At present, we lack an absolute calibration for these r'-band Mosaic-II data. All apparent magnitudes cited in this paper are a pipeline calibration product (see Section 2.3). They are to be considered rough estimates and thereby used with caution until secondary standards are established for the Mosaic-II fields. The pipeline zero-point calibration carries an estimated uncertainty of 0.5 mag.

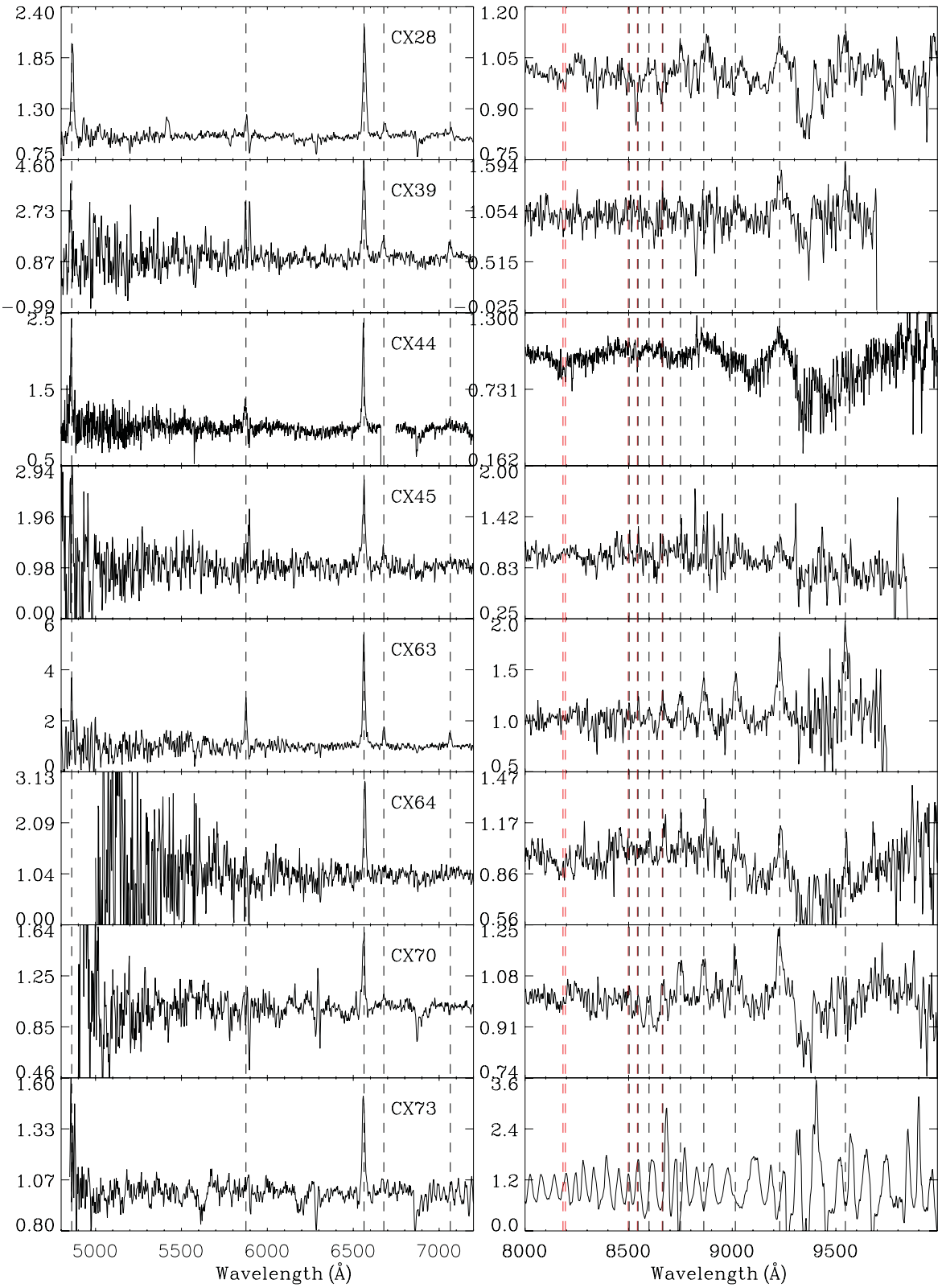

Figure 1. Continuum-normalized spectra of GBS sources in two wavelength ranges. The rest wavelengths for the lines given in Section 3.1 are marked with black dashed lines except the Ca II IR triplet (red dashed lines in online version). Note that the P13, 15 and 16 Paschen lines are blended with the Ca triplet.

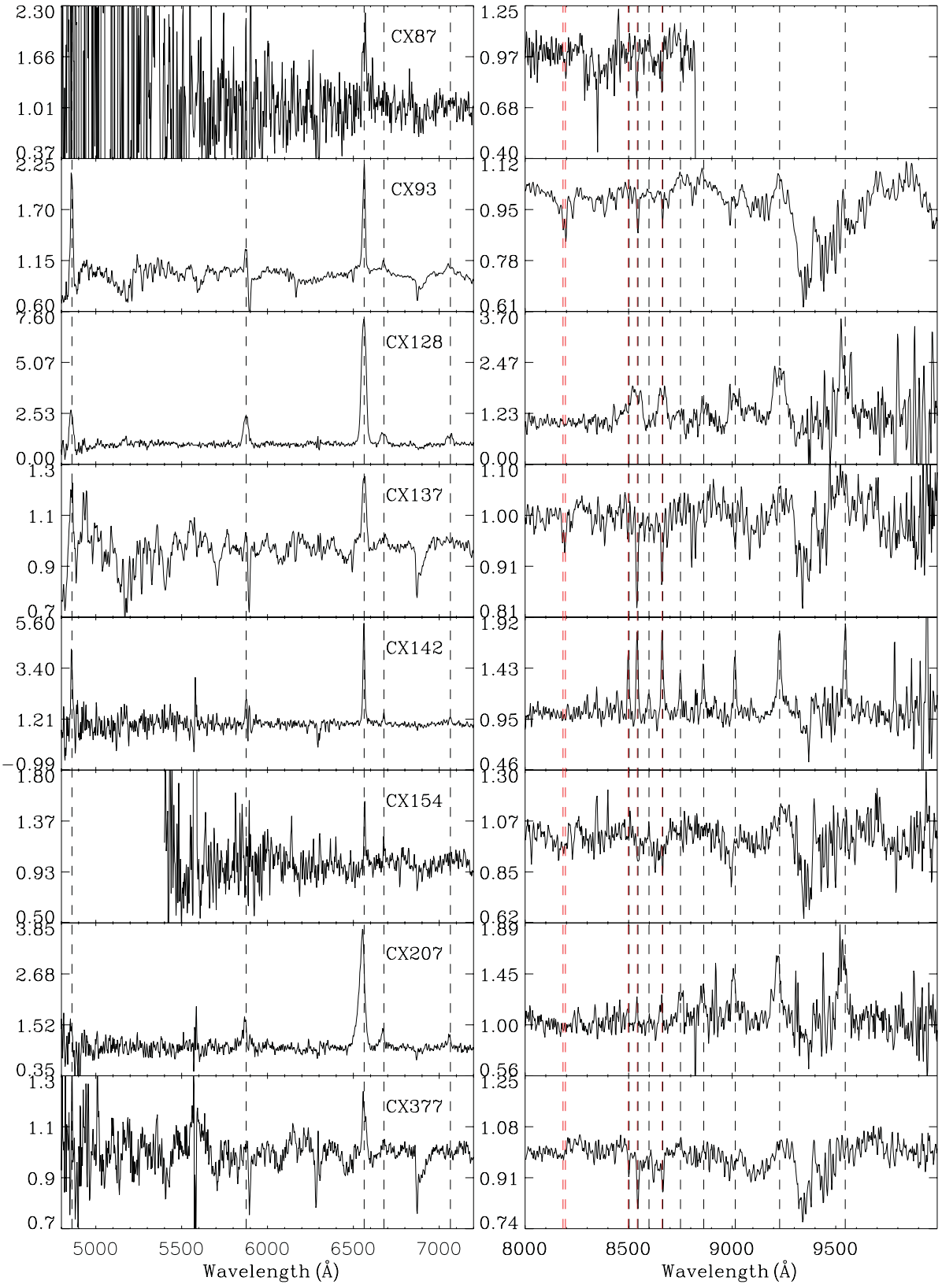

Figure 2. Normalized spectra of GBS sources (continued from Fig. 1).

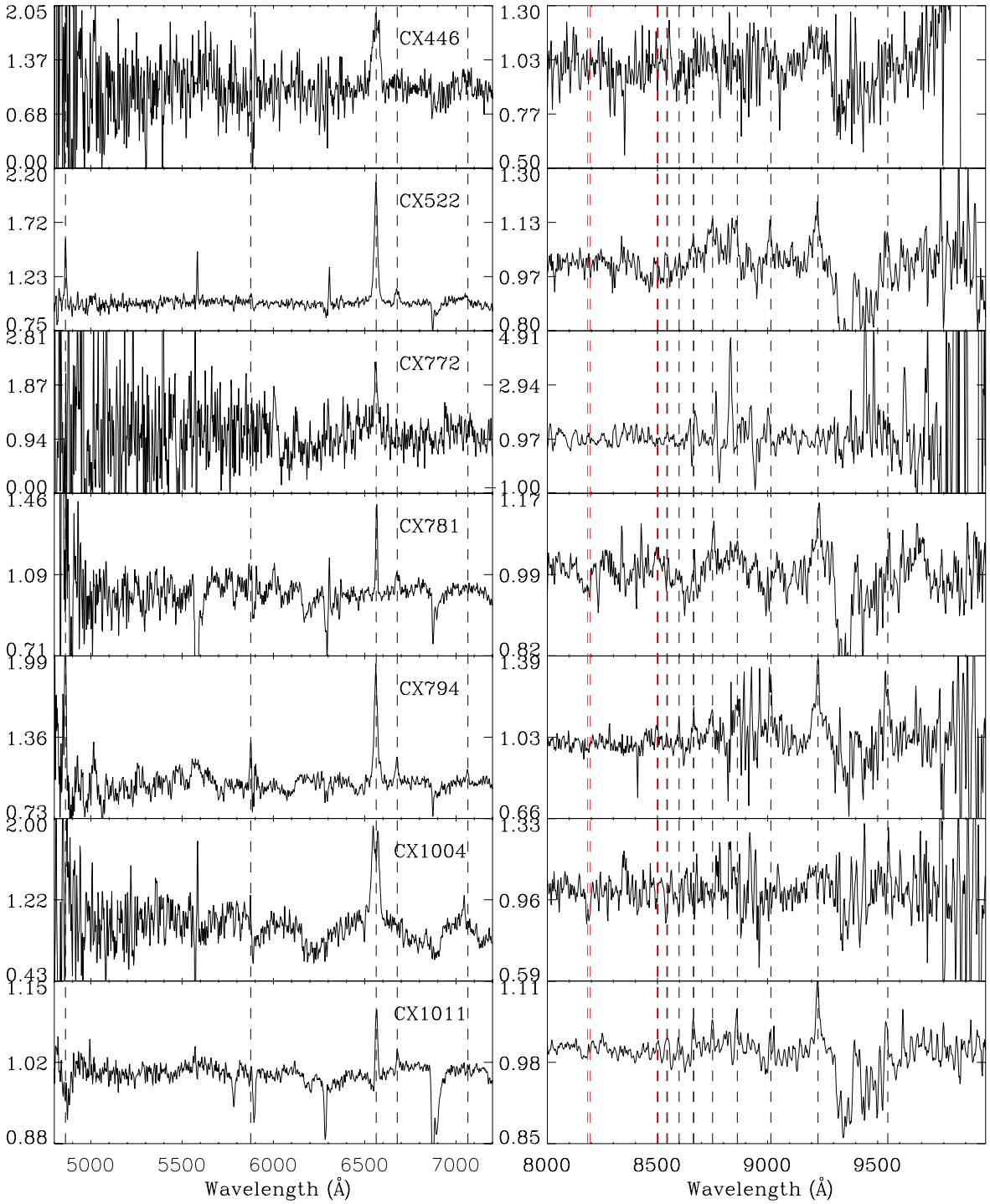

Figure 3. Normalized spectra of GBS sources (continued from Fig. 2).

4 RESULTS AND DISCUSSION

4.1 Criteria for the spectroscopic identification of accreting binaries

All counterparts were selected for showing (at least) Hα in emission above the continuum. A key motivation of this work is to report the secure and likely accreting binaries found in this sample and describe the selection criteria used for their identification. We will report on additional candidate counterparts to X-ray sources that showed no Hα emission line in their spectrum elsewhere (see e.g. Hynes et al. 2014).

Typically, accreting binaries with hydrogen-rich mass donor stars are unambiguously identified by the presence of broad hydrogen and helium emission lines formed in the gas being accreted. Emission from this gas and/or from a white dwarf primary (in the case of CVs) produces a characteristic excess in the optical continuum at blue wavelengths. We have based the identification of accreting binaries on the detection of strong (EW $>$ 18 Å, see below) Hα in emission, the Doppler-broadening of the hydrogen line profiles or

Table 2. Spectroscopic measurements. An * indicates that the measured EW is most likely a lower limit due to contamination of unresolved star/s during the extraction of the spectra.

GBS ID Line	RV (km s^{-1})	EW (Å)	FWHM (Å)
CX28*			
He II 4686	420 ± 30	23 ± 3	19.2 ± 0.7
H I 4861	320 ± 20	13.4 ± 0.5	14.3 ± 0.5
He II 5412	330 ± 20	5.1 ± 0.3	22.3 ± 0.7
He I 5876	150 ± 20	3.9 ± 0.1	16.1 ± 0.3
H I 6562	150 ± 10	22.5 ± 0.9	19.8 ± 0.2
He I 6678	300 ± 20	3.4 ± 0.5	21.4 ± 0.2
CX39*			
H I 6562	−5 ± 4	86 ± 4	20 ± 1
He I 6678	151 ± 9	15 ± 1	21.2 ± 0.8
He I 7065	−50 ± 20	11.4 ± 0.5	19.4 ± 0.7
CX44			
H I 4861	−190 ± 20	11 ± 1	9 ± 2
He I 5876	−170 ± 40	5.8 ± 0.5	21.0 ± 0.7
H I 6562	−240 ± 9	20 ± 1	13.4 ± 0.1
CX45			
H I 6562	−48 ± 4	40 ± 3	21.6 ± 0.3
He I 6678	−2 ± 16	8.5 ± 0.2	20.9 ± 0.9
CX63*			
H I 4861	−63 ± 4	$\gtrsim$35 ± 2	$\gtrsim$9 ± 1
He I 5876	−13 ± 5	31 ± 8	12.1 ± 0.9
H I 6562	−45 ± 2	65 ± 2	14.8 ± 0.1
He I 6678	13 ± 4	9.8 ± 0.1	13.4 ± 0.5
He I 7065	−60 ± 10	9.0 ± 0.3	14.6 ± 0.5
H I 8665 (P13)	−30 ± 10	4.7 ± 0.9	20.8 ± 0.9
H I 8750 (P12)	−2 ± 7	8.8 ± 0.4	23.5 ± 0.9
H I 8862 (P11)	50 ± 30	14.6 ± 2.4	32 ± 4
H I 9015 (P10)	50 ± 20	9.6 ± 1.7	22.0 ± 0.9
H I 9229 (P9)	−30 ± 6	18.1 ± 0.7	28.1 ± 0.5
CX64			
H I 6562	212 ± 2	33 ± 1	14.8 ± 0.1
CX70			
H I 6562	−133 ± 2	15 ± 1	20.3 ± 0.2
H I 8598 (P14)	−70 ± 20	2.9 ± 0.1	25.0 ±0.2
H I 8665 (P13)	61 ± 7	3.6 ± 0.3	23 ± 2
H I 8750 (P12)	−90 ± 10	4.0 ± 0.2	27.6 ± 0.8
H I 8862 (P11)	30 ± 40	3.6 ± 0.4	25 ± 1
CX73			
H I 6562	−116 ± 4	11.4 ± 0.2	18.8 ± 0.4
CX87			
H I 6562	50 ± 50	24 ± 5	27 ± 3
CX93			
H I 4861	−70 ± 20	27 ± 2	16.7 ± 0.2
He I 5876	−60 ± 10	5.0 ± 0.5	15.5 ± 0.4
H I 6562	−17 ± 4	18.4 ± 0.3	16.7 ± 0.3
He I 6678	−64 ± 2	1.6 ± 0.2	18.2 ± 0.4
CX128*			
H I 4861	−180 ± 60	91 ± 5	26.2 ± 0.8
He I 5876	−30 ± 20	56 ± 5	33 ± 1
H I 6562	−70 ± 4	197 ± 7	31.0 ± 0.2
He I 6678	−180 ± 10	20 ± 1	35.5 ± 0.4
He I 7065	−110 ± 40	20 ± 1	44 ± 4
H I 8545 (P15)	−180 ± 10	69 ± 7	61 ± 4
H I 8665 (P13)	−20 ± 10	48 ± 4	46.6 ± 0.7
H I 9015 (P10)	−130 ± 30	45 ± 2	58 ± 3
H I 9229 (P9)	−40 ± 20	100 ± 30	65 ± 3
CX137*			
H I 6562	−9 ± 9	$\gtrsim$6.5 ± 0.2	$\gtrsim$23.4 ± 0.4

Table 2 – *continued*

GBS ID Line		RV (km s^{-1})	EW (Å)	FWHM (Å)
CX142				
H I 4861		−90 ±10	120 ± 80	14 ± 2
He I 5876		—	—	—
H I 6562		−69 ± 1	59 ± 4	12.4 ± 0.2
He I 6678		−28 ± 9	4.9 ± 0.3	9 ± 1
He I 7065		−42 ± 8	6.2 ± 0.4	16.0 ± 0.9
Ca II 8498 + P16		0 ± 10	8.0 ± 0.4	10.4 ± 0.3
Ca II 8542 + P15		−39 ± 2	10.8 ± 0.3	1.1 ± 0.3
H I 8598 (P14)		−10 ± 20	4.2 ± 0.6	13.3 ± 0.5
Ca II 8662 + P13		−7 ± 2	9.2 ± 0.3	11.1 ± 0.4
H I 8750 (P12)		−37 ± 7	4.8 ± 0.2	11.0 ± 0.3
H I 8862 (P11)		−68 ± 7	7 ± 1	14 ± 2
H I 9015 (P10)		−54 ± 7	8.0 ± 0.4	12.8 ± 0.7
H I 9229 (P9)		−31 ± 7	11 ± 1	17 ± 1
H I 9546 (P8)		−44 ± 7	10.2 ± 0.6	13.6 ± 0.2
CX154*		(1,2: 2011 May 26, Jun 9)		
H I 6562	1	95 ± 9	8 ± 2	11.3 ± 0.8
	2	142 ± 4	7.6 ± 0.4	8.5 ± 0.5
He I 6678	2	10 ± 9	2.8 ± 0.4	12.7 ± 0.4
CX207*		(1,2: 2011 May 2, Jun 6)		
He I 5876	1	−370 ± 20	14 ± 2	22 ± 1
	2	−210 ± 50	21 ± 2	41 ± 4
H I 6562	1	−558 ± 4	107 ± 8	37.7 ± 0.7
	2	−358 ± 4	83 ± 9	35.1 ± 0.6
He I 6678	1	−330 ± 10	10 ± 1	22.0 ± 0.8
	2	−200 ± 100	7 ± 1	32 ± 5
He I 7065	1	−250 ± 10	6.8 ± 0.6	22 ± 2
	2	−190 ± 30	6.5 ± 0.3	38 ± 2
H I 8665 (P13)	1	−280 ± 10	3.2 ± 0.4	16 ± 1
H I 8862 (P11)	1	−200 ± 30	8 ± 3	29 ± 3
H I 9015 (P10)	1	−280 ± 20	7.7 ± 0.9	19.5 ± 0.8
H I 9229 (P9)	1	−330 ± 30	23 ± 6	39 ± 8
	2	−180 ± 30	33 ± 3	55 ± 3
H I 9546 (P8)	1	−460 ± 30	37 ± 9	46 ± 2
CX377*		(1,2: 2011 Jul 23, Aug 28)		
H I 6562	1	30 ± 30	6.6 ± 0.3	29 ± 2
	2	−39 ± 4	6.4 ± 0.2	27.3 ± 0.6
CX446				
H I 6562		−10 ± 20	50 ± 4	49 ± 1
CX522				
e H I 4861		42.0 ± 0.1	6 ± 1	10 ± 1
He I 5876		30 ± 70	1.2 ± 0.2	16 ± 3
H I 6562		−84 ± 1	23.3 ± 0.9	21.1 ± 0.2
He I 6678		−80 ± 40	3.2 ± 0.3	25 ± 2
CX772				
H I 6562		−40 ± 20	24 ± 4	22 ± 4
CX781				
H I 6562		102 ± 1	5.0 ± 0.2	10.1 ± 0.2
He I 6678		10 ± 30	2.3 ± 0.2	24 ± 2
CX794				
H I 4861		−10 ± 10	13 ± 1	9.8 ± 0.7
H I 6562		−69 ± 4	23 ± 1	23.0 ± 0.4
He I 6678		−80 ± 20	5 ± 2	19 ± 2
CX1004				
H I 6562		−210 ± 20	32.9 ± 0.4	46.4 ± 0.4
CX1011		(1,2: 2011 May 13, Jun 28)		
H I 6562	1	18 ± 6	2.36 ± 0.04	13.59 ± 0.04
	2	93 ± 5	2.14 ± 0.07	15.1 ± 0.2
He I 6678	2	40.2 ± 10	0.46 ± 0.04	13.3 ± 0.5
H I 9229 (P9)	2	50 ± 10	1.5 ± 0.1	16.7 ± 0.5

the detection of He I λ6678 emission in the case of observing weak and narrow hydrogen lines. A search for carbon, nitrogen and oxygen emission lines was also performed. Emission from these heavy elements in a spectrum lacking hydrogen lines is observational evidence for a carbon–oxygen white dwarf donor in an ultracompact X-ray binary (see e.g. Nelemans et al. 2004; Nelemans, Jonker & Steeghs 2006; Werner et al. 2006). None were found so far in our sample.

Chromospherically active binaries and stars can be distinguished from qLMXBs and low accretion rate CVs by the presence of Hα emission that does not exceed 15–18 Å in EW. This limit is observed in M-type stars (Mohanty & Basri 2003; Covey et al. 2008) and post-common envelope binaries (Bleach et al. 2002), but does not account for the possibility of finding larger EWs during a flare event. In active stars, line broadening of the Hα profile can be well above the rotational broadening measured in the photospheric lines and reach up to 9 Å (= 400 km s^{-1}) FWHM in extremely active objects (see e.g. Walter & Basri 1982; Torres et al. 2005). The lack of helium in emission above the continuum is also a common characteristic of chromospherically active sources. Out of a flare, He I emission above the continuum has been found in a few very active objects (see Bleach et al. 2002 and references therein). From Bleach et al., one can establish that when present in emission, the He I λλ5876, 6678 lines do not exceed 3 Å in EW. The He I to Hα line ratios are $<$0.2 even during flares.

Pre-main-sequence stars that host a circumstellar disc (Classic T Tauri stars) may show permitted lines in emission and mimic the optical and X-ray characteristics of reddened CVs and qLMXBs at a low accretion rate state. For instance, they can reach X-ray luminosities of up to 10^{31} erg s^{-1} (Telleschi et al. 2007), a value typically observed in quiescent black hole LMXBs, and their optical spectra can exhibit broad hydrogen lines that can appear asymmetric or double peaked and have EWs of hundreds of Å (e.g. Hamann & Persson 1992; Reipurth, Pedrosa & Lago 1996; Barrado y Navascués & Martín 2003). Helium lines are often present in the optical spectrum. Fortunately, this young class of objects can be identified on the basis of their association with star formation regions.

4.2 Application to the current sample

Through the analysis of the VIMOS and IMACS spectroscopy, we have found optical counterparts to 54 GBS sources. Of the 52 optical counterparts with an Hα emission line found in the data, 29 of them are likely chromospherically active objects as they show narrow (unresolved) Hα emission with EW $<$ 3 Å and a continuum clearly marked by absorption features from a late-type star or binary components.[1] Using the SIMBAD data base, we have not found known star-forming regions, star clusters, OB associations or H II regions within 1 arcmin radius of any of the 23 remaining sources. Applying the aforementioned EW limit of 18 Å, 15 of the 23 sources are classified as accreting binaries. Six of the remaining eight objects (CX70, CX73, CX93, CX137, CX377 and CX1011) have Hα profiles with FWHM ranging from 15 to 30 Å. When subtracting in quadrature the instrumental width, they correspond to intrinsic broadenings of 11–28 Å (∼500–1300 km s^{-1}). Such values are above the 9 Å maximum broadening observed in chromospherically active sources. This indicates that the line profiles in these sources are broadened due to the motion of emitting material in an accretion flow or wind. Finally, the GBS sources CX154 and CX781 qualify as likely accreting binaries on the basis of the presence of He I λ6678 in emission with a He I/Hα ratio above the value expected from lines powered by chromospheric activity. Thus, we conclude that all 23 sources are most likely accreting binaries.

[1] These sources will be presented elsewhere once their chromospheric active nature is fully established through further analysis and/or observation. The objects in question are CX25, 29, 47, 57, 74, 124, 126, 161, 251, 294, 321, 325, 381, 393, 409, 450, 469, 502, 634, 642, 712, 820, 852, 858, 881, 895, 1014, 1088 and 1169.

4.3 Further constraints on binary parameters from emission-line properties

The measured emission-line properties provide not only a method to discern accreting binaries from other classes of objects, but also encode a wealth of information on binary parameters such as the system inclination, orbital period, compact object nature or mass accretion rate (see e.g. Warner 1995). In particular, the centroid of the line profiles originating in a disc with gas in Keplerian motion will be shifted by the systemic and primary's radial velocities at the time of the observation: $\gamma + K_1 \sin\phi$, where ϕ is the orbital phase, K_1 the RV semi-amplitudes of the primary and γ is the systemic RV. Additional velocities incurred by the gas motion in the accretion disc may be present as well. Furthermore, the line broadening scales with the mass of the compact object, the system inclination and the orbital period as $(M_1/P_{\rm orb})^{1/3} \sin i$. In this regard, the low intrinsic FWHM of the Hα line in CX44 (510 km s^{-1}) suggests a moderate to low inclination for this system and thereby a low K_1. Thus, the large RV offset in the emission lines ($|RV| \sim 200$ km s^{-1}) likely reflect a high γ given that the RV component due to the motion of the primary is expected to be low. On this basis, CX44 is a good candidate for an LMXB that experienced a natal kick – CVs in general have low γ (van Paradijs, Augusteijn & Stehle 1996; Ak et al. 2010). The line profiles in CX207 and CX1004 have also significant RV offsets and exhibit the highest line broadening in the sample (FWHM $>$1600 km s^{-1}) in favour of a high inclination for both binaries (both sources are discussed below). However, caution must be taken with this interpretation of the line properties as departures for the simplistic picture of a Keplerian disc are expected and can be dominating the observed RV*and* FWHM. For instance, complexities in the line profile morphology can result from tidal effects on the disc (Foulkes et al. 2004) and winds that will cause asymmetric profiles. Also, emission originating in regions of the binary system other than the disc can contribute or even dominate the line profile shape and variability. For instance, this is the case in highly magnetic CVs (known as polars) where the magnetic field of the white dwarf prevents the formation of an accretion disc. Emission lines in these systems can originate from the accretion stream that is directed towards the white dwarf's magnetic poles and from the (irradiated) donor star. As discussed below, a highly magnetic CV is the favoured scenario to explain the emission-line properties in CX207.

5 INDIVIDUAL OBJECTS

In what follows, we discuss the spectroscopy and photometry of the 23 accreting binaries. We describe remarkable features and provide a characterization of the GBS source on their basis. When useful we will employ the absolute magnitudes and colours of stars as given in Allen's Astrophysical Quantities (Cox 2000) and apply the transformation equations between Johnson–Cousins and SDSS magnitude derived by Jester et al. (2005) and Bilir, Karaali & Tunçel (2005). We will quote from Jonker et al. (2011) the X-ray harness

ratio or/and the number of counts detected in the 0.3–8 keV band during the discovery observations with *Chandra*. The hardness ratio is defined as HR = $(H-S)/(H+S)$, where S and H are the soft 0.3–2.5 keV and hard 2.5–8 keV band count rates. We provide here counts to 0.5–10 keV unabsorbed flux conversion factors of 6.6×10^{-15} and 1.4×10^{-14} erg cm^{-2} s^{-1} count^{-1}. They were obtained using a power-law spectra with index $\Gamma = 2$ modified by a Galactic absorption column density $N_{\rm H}$ of 10^{21} and 10^{22} cm^{-2}, respectively. The adoption of this spectral shape for the X-ray sources yields a rough but useful conversion except for soft sources suffering significant reddening in which case the flux will be underestimated by a factor of ∼10. Additionally, we give expressions to compute the unabsorbed 0.5–10 keV X-ray luminosity as a function of the distance to the source d and the X-ray counts: $L_{\rm x}(d, N_{\rm H} = 10^{21}) = 7.9 \times 10^{29} \times$ counts $\times (\frac{d}{1.0\,{\rm kpc}})^2$ and $L_{\rm x}(d, N_{\rm H} = 10^{22}) = 1.6 \times 10^{30} \times$ counts $\times (\frac{d}{1.0\,{\rm kpc}})^2$ erg s^{-1}. In general, we will adopt $N_{\rm H} = 10^{21}$ cm^{-2} for objects lacking clear detection of DIBs. The inferred luminosities are below those observed in very faint persistent neutron star LMXBs (e.g. Armas Padilla, Degenaar & Wijnands 2013) and within the broad range of luminosities observed in CVs (Baskill, Wheatley & Osborne 2005; Byckling et al. 2010; Reis et al. 2013) and qLMXBs (see e.g. Jonker et al. 2012).

CX28 = CXOGBS J173946.9−271809, a high accretion rate CV

Results based in part on the VIMOS spectrum (Fig. 1) and the Mosaic-II time-resolved photometry suggest that CX28 is a high accretion rate CV. This classification is supported by the detection of the high-excitation emission line He II λλ4686, 5412. We refer the reader to Britt et al. (2013) for a full discussion. The absorption lines detected at λλ8349, 8536, 8659 in the VIMOS spectrum are caused by contamination of a late type field star NE from this GBS source. A finding chart for the optical counterpart to CX28 can be found in Britt et al. (2013) as well.

CX39 = CXOGBS J174140.0−271738, an outbursting CV

The VIMOS spectrum of CX39 (Fig. 1) exhibits Hα and He I λλ6678, 7065 emission with single-peaked asymmetric line profiles of intrinsic FWHM ranging from 700 to 840 km s^{-1}. Note here that the apparent narrow emission features near λ5900 are sky-line residuals. Photospheric lines from the donor star are not obvious in the spectrum. The presence of DIBs at λλ6284, 8620 is uncertain. The soft X-ray hardness ratio HR = -0.35 ± 0.25 indicates low reddening and thereby a nearby object.

The optical light curve (Fig. 4) shows, what appears to be a brief outburst of 1.2 mag amplitude, rising on the first day of observations and decaying to $r' = 20.2$ over the next 3 d. After that, the counterpart flickers with an rms scatter of 0.1 mag. We examined the spatial profile of both the optical counterpart spectrum and the spectra of field stars contained in the slit. This together with comparison of the VIMOS pre-images obtained on 2010 Mar 31 and Aug 17 UT shows that CX39 was not in outburst during the spectroscopic observations.

Recurrent low-amplitude brightenings with fast return to minimum light have been observed in the long-term light curves of dwarf novae (see e.g. Shears, Boyd & Poyner 2006) and with lower amplitude in nova-like CVs (Rodríguez-Gil et al. 2012b). In addition, a small number of weak magnetic CVs (intermediate polars, IPs) are known to undergo relatively short duration and low-amplitude outbursts (see e.g. Ishioka et al. 2002, and references therein).

The lack of stellar features in the quiescent optical spectrum together with this photometric behaviour suggests that CX39 is a dwarf nova or IP with a disc-dominated optical spectrum. The X-ray flux detected with *Chandra* (36 counts) implies $L_{\rm x}(d, N_{\rm H} = 10^{21}) = 2.8 \times 10^{31} \times (\frac{d}{1.0\,{\rm kpc}})^2$ erg s^{-1}.

CX44 = CXOGBS J175542.8−281809 = AX J1755.7−2818, a qLMXB or a low accretion rate CV

The IMACS spectrum of CX44 (Fig. 1) shows Hα and Hβ in emission. He I λ5876 is present while the location of the He I λ6678 line fell in a chip gap. The IMACS spectrum also covers the high-excitation line He II λ4686, which is not detected. As reported in Section 4.2, the emission lines exhibit velocity offsets of about −200 km s^{-1}. Moreover, photospheric features from a K-type companion star are visible in the spectrum, the strongest being the molecular bands of the TiOγ' system situated longward of λ5840, Ca I λ6162 and the blend of Fe I + Ca I at rest wavelength λ6495. Gaussian fits to the metal-line profiles yield a −50 km s^{-1} RV. In the red, the spectrum is dominated by numerous telluric features and shows evidence for absorption from the Ca II λ8542 line. There is no obvious detection of the Na I λ8190 doublet or Paschen lines (neither in emission nor in absorption). The lack of strong photospheric lines from the donor in this part of the spectrum suggests a significant contribution to the *I*-band continuum by the accretion disc.

The optical light curve (Appendix A) shows aperiodic variability with an rms of 0.05 mag. and with an observed maximum variability of $\Delta r' = r'_{\rm max} - r'_{\rm min} = 0.2$ mag.

CX44 is the unique GBS source within the 50 arcsec-radius error circle of AX J1755.7−2818. This ASCA object was found at a 0.7–10 keV flux level of 1.2×10^{-12} erg cm^{-2} s^{-1} during a pointing observation on 1999 Nov 2 (Sakano et al. 2002). 32 counts were observed from CX44 with *Chandra* on 2008 May 4. Using an absorbed power-law model with $\Gamma = 2$ and $N_{\rm H}$ ranging from 10^{21} to 10^{22} cm^{-2}, we derive an absorbed flux of $(1.7–2.5) \times 10^{-13}$ erg cm^{-2} s^{-1} in the 0.7–10 keV band. This flux is at least five times lower than the value found during the ASCA observation.

Given the lack of strong DIBs in the optical spectrum and the soft X-ray hardness ratio (HR = -0.19 ± 0.19), we expect CX44 to be a nearby (few kpc) binary with a non-evolved donor star. From the apparent optical magnitude ($r' = 18.7$), we obtain a rough estimation of 2 kpc for its distance by assuming a K5 V companion star ($M_{r'} = 7.0$) and by neglecting both the effects of interstellar reddening and veiling from the accretion disc. We also derive $L_{\rm x}(d, N_{\rm H} = 10^{21}) \sim 1 \times 10^{32} \times (\frac{d}{2.0\,{\rm kpc}})^2$. This X-ray brightness of the source together with, the detection of the donor star and the dominant flickering in the optical light curve suggests that we may have found a nearby low accretion rate CV or a quiescent neutron star LMXB where the accretion disc contributes in a large fraction to the optical light.

CX45 = CXOGBS J173538.5−285251, a CV with an accretion-dominated optical spectrum

The VIMOS spectrum of CX45 (Fig. 1) shows Hα and He I λ6678 emission. The profiles for both lines are asymmetric and have an intrinsic ≈900 km s^{-1} (FWHM) broadening. The narrow emission features near λ5900 are sky-line subtraction residuals. Longward of Hα there are no obvious emission lines. There is no clear detection

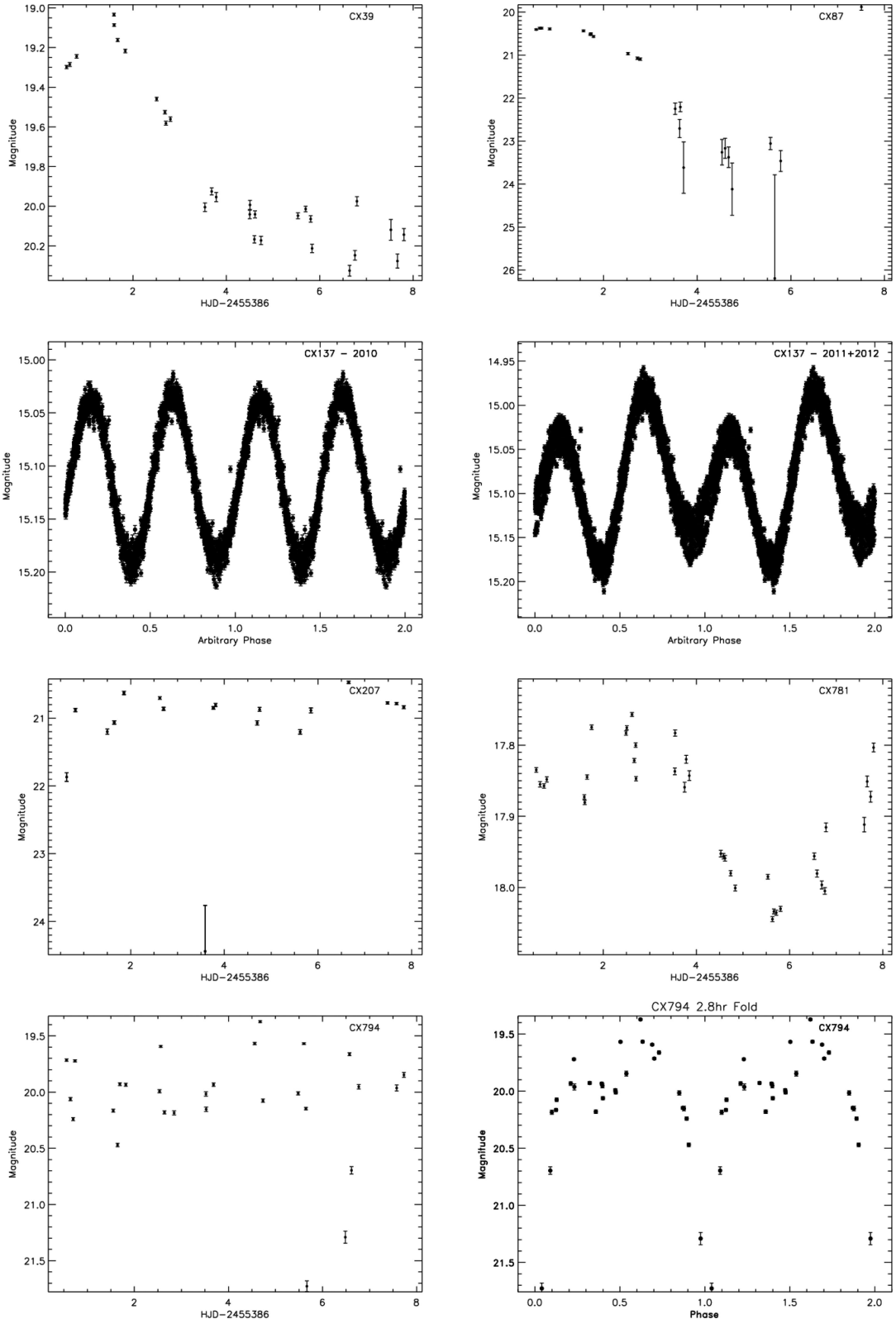

Figure 4. Optical light curves for sources that undergo outburst or show a photometric modulation including eclipses. The CX137 light curves are based on OGLE-IV data The Mosaic-II light curve of CX794 is also shown folded on the ephemeris of Section 5.

of absorption features from the donor star in the full spectral range covered by VIMOS. The Mosaic-II light curve (Appendix A) shows flickering with an rms scatter of 0.4 mag. The amplitude of the observed variability is large: $\Delta r' = 1.5$ mag.

The strong flickering at optical wavelengths together with the apparent lack of photospheric lines from the donor star supports that CX45 is a CV in a state of high mass transfer rate. Alternatively, CX45 could be a low accretion rate CV with the optical spectrum dominated by emission from the accreting flow as for instance observed in short orbital period dwarf novae (see CX128 for more discussion on this type of CVs). The brightness of the X-ray source (32 counts in the *Chandra* detection, HR $= 0.66 \pm 0.24$) yields $L_{\rm x}(d, N_{\rm H} = 10^{21}) = 2.5 \times 10^{31} \times (\frac{d}{1.0\,{\rm kpc}})^2$.

CX63 = CXOGBS J173411.3−293117, a CV with an accretion-dominated optical spectrum

The optical spectrum of CX63 (Fig. 1) is dominated by the accretion disc, there are no signs of photospheric lines from the donor star. Hα and He I $\lambda\lambda$5876, 6678, 7065 are in emission with intrinsic broadening between 350 and 500 km s^{-1} (FWHM). Hβ is also present and appears to be unresolved. In the red, P8–P13 emission lines are seen. The intrinsic broadening for the Paschen lines ranges from 630 to 1000 km s^{-1} (FWHM).

The optical light curve of CX63 (see Appendix A) displays events of increased/decreased brightness of up to 0.5 mag from its 21.3 mean magnitude. The rms scatter in the Mosaic-II photometry is 0.16 mag, while $\Delta r' = 0.85$ mag.

CX63 is bright in X-rays with 26 counts detected with *Chandra* (HR $= 0.16 \pm 0.23$, $L_{\rm x}(d, N_{\rm H} = 10^{21}) = 2.1 \times 10^{31} \times (\frac{d}{1.0\,{\rm kpc}})^2$). The characteristics of the optical spectrum together with the flickering observed in the light curve support that CX63 is a high accretion rate CV or a low accretion rate CV with an accretion-dominated optical spectrum The low FWHM values measured from the emission-line profiles support a moderate to low-inclination system.

CX64 = CXOGBS J173802.7−283126, a CV in a low state of accretion or a CV in the bulge region

The Hα emission line (intrinsic FWHM $= 500 \pm 10$ km s^{-1}) is the only feature detected in the blue part of the VIMOS spectrum of CX64 (Fig. 1). The line profile appears to be redshifted by 200 km s^{-1}. Longward of Hα, lines of the Paschen series may be in emission. It is unclear whether DIBs or photospheric lines from the donor star are present due to the noise in the spectrum. The optical counterpart to CX64 is faint with $r' = 22.3$. The Mosaic-II light curve (Appendix A) allows us to place an upper limit in the photometric variability of 0.14 mag (rms).

If Hα is originated in the accretion disc, its low intrinsic broadening implies a moderate to low system inclination and thereby K_1. Given the moderate K_1 and that CVs are expected to have low systemic velocities (see CX207 below for more details), the large velocity offset observed in the line can be explained if CX64 is a bulge CV (accreting at high mass transfer rate). On the other hand, both the RV offset and low line broadening are also consistent with a more nearby CV in a low state. High accretion rate CVs in a low state of mass transfer show narrow emission lines originating in the irradiated donor stars. The radial velocities of these lines reflect therefore the motion of the donor star. The non-detection of He I λ6678 in the optical spectrum of CX64 is in support of this possibility as magnetic and nova-like CVs have shown weak He I λ6678 or absence of the line during low-state periods (e.g. Kafka et al. 2005; Rodríguez-Gil et al. 2012a). Unfortunately, we cannot confirm this scenario as we lack the signal to search for absorption features from the stellar components. On the basis of the X-ray brightness (25 *Chandra* counts, HR $= 0.22 \pm 0.23$), we derive $L_{\rm x}(d, N_{\rm H} = 10^{21}) = 2.0 \times 10^{31} \times (\frac{d}{1.0\,{\rm kpc}})^2$ erg s^{-1}.

CX70 = CXOGBS J173535.1−295942, a CV with an accretion-dominated optical spectrum

The spectrum of the optical counterpart to CX70 shows the Hα and P10–P15 hydrogen lines in emission with intrinsic broadening of ∼700–900 km s^{-1} (see Fig. 1 and line parameters in Table 2). The presence of He I λ6678 is uncertain as the line position fell on a region of bad rows in the detector. While artefact features make difficult to address the presence of photospheric lines and DIBs in the blue part of the spectrum, it is clear that stellar lines are not present at wavelengths redward of λ8000.

The Mosaic-II light curve (Appendix A) shows significant variability with an rms of 0.07 mag and $\Delta r' = 0.3$ mag. A Lomb–Scargle periodogram yields a peak at a period of 5.6 h. However, we find a false alarm probability of 7.8 per cent for this period by running Monte Carlo simulations on randomly ordered light curves.

The non-detection of absorption features from the donor star and the photometric flickering suggest a high accretion rate CV or a CV accreting at lower mass transfer rate, but having an accretion-dominated optical spectrum. From the X-ray brightness (24 counts, HR $= 0.63 \pm 0.29$), we obtain $L_{\rm x}(d, N_{\rm H} = 10^{21}) = 1.9 \times 10^{31} \times (\frac{d}{1.0\,{\rm kpc}})^2$ erg s^{-1}.

CX73 = CXOGBS J174447.5−270101

The only emission line detected in the optical spectrum of CX73 (Fig. 1) is Hα with an intrinsic FWHM of 730 ± 20 km s^{-1}. As in CX70 it is difficult to confirm or reject evidence for absorption lines in the blue part of the spectrum. The red part of the data is strongly affected by fringing since the observations were taken before the VIMOS detector upgrade (see Section 2.1).

The Mosaic-II light curve (Appendix A) shows aperiodic variability with an rms scatter of 0.08 mag and $\Delta r' = 0.3$ mag. This variability supports a significant contribution from the accretion flow to the optical light. Spectroscopic observations (for instance in the *I* band) are necessary to further constrain the nature of CX73. An X-ray luminosity of $L_{\rm x}(d, N_{\rm H} = 10^{21}) = 1.8 \times 10^{31} \times (\frac{d}{1.0\,{\rm kpc}})^2$ erg s^{-1} is derived from the 23 counts (HR $= 0.22 \pm 0.25$) detected with *Chandra*.

CX87 = CXOGBS J173648.1−293639, an outbursting CV

The VIMOS spectrum of the optical counterpart to CX87 can be found in Fig. 2. Due to its low signal-to-noise ratio, we only detect Hα in emission with FWHM $= 1150 \pm 140$ km s^{-1} and EW $= 24 \pm 5$ Å. The line profile appears double peaked with a peak-to-peak velocity separation of $\Delta v = 650 \pm 80$ km s^{-1}.

The Mosaic-II light curve (Fig. 4) shows the source declining in brightness by 2.9 mag, reaching minimum brightness ($r' \sim 23$) four days after the first photometric observation. Examination of the VIMOS pre-image taken on 2011 Mar 30 UT and the spatial profile of the optical counterpart in the VIMOS spectrum show that CX87 was most likely in quiescence during the Very Large Telescope observations.

It is likely that the Mosaic-II photometry was obtained during the final stage of a CV outburst that brightened by more than 2.9 mag

at optical wavelengths. This would support a dwarf nova nature for CX87. Alternatively, CX87 could be an outbursting IP. Some IPs have outbursts with a 3–5 mag amplitude and a few days duration (see e.g. Ishioka et al. 2002). The X-ray flux observed with *Chandra* (21 counts, HR = 0.31 ± 0.25) implies $L_{\rm x}(d, N_{\rm H} = 10^{22}) = 3.0 \times 10^{32} \times (\frac{d}{3.0\,{\rm kpc}})^2$ erg s^{-1}.

CX93 = CX153 = CXOGBS J174444.6−260328, a low accretion rate CV

CX93 is a 0.237 d orbital period CV observed at a low accretion rate state. A complete dynamical study of this source is presented in Ratti et al. (2013a). The VIMOS data for CX93 are analysed in Ratti's work, and therefore, we will not discuss them further except for the following erratum: the EWs measured for the Hα emission line in the VIMOS spectra are incorrect. Correct values can be found in this work (Table 2). As a consequence the claim in Ratti et al. of a more active state of accretion at the time of the VIMOS observations must be disregarded. A finding chart for the field of CX93 can also be found in Ratti's work.

CX128 = CXOGBS J174028.3−271136, a likely short orbital period dwarf nova

The emission-line spectrum of CX128 (Fig. 2) shows very strong Hα and Hβ emission lines with single-peaked profiles with an intrinsic FWHM of ∼1400 km s^{-1}. He I λλ5876, 6678, 7065 are also in emission with similar broadening, though they appear double peaked. He I λ5876 is the stronger of these three lines. At longer wavelengths CX128 shows emission lines of the Paschen series. The lines are broad (1500–2100 km s^{-1} FWHM) with complex (multi-peaked) profiles. Neither photospheric lines nor interstellar bands are detected indicating that light from the accreted material dominates and that the source suffers moderate reddening. The Mosaic-II photometry (Appendix A) shows flickering of 0.3 mag rms and $\Delta r' = 0.9$.

The lack in the spectrum of underlying features from the donor can be explained if this GBS source is a high accretion rate (nova-like or magnetic) CV. However, the EWs for the Balmer and helium lines (Table 2) seem high compared to those observed in nova-like CVs (Dhillon 1996; Rodríguez-Gil, Schmidtobreick & Gänsicke 2007a; Rodríguez-Gil et al. 2007b). Furthermore, we do not detect emission from He II λ5412, a signature that would have been sufficient to confirm the above scenario. An alternative possibility is that CX128 is a dwarf nova CV below the period gap in quiescence at the time of our observations. In this scenario, the contribution from the small donor star to the optical light is veiled by the accretion disc and the spectrum shows only emission lines. Examples of such spectra can be found in the dwarf novae SS UMa, SU UMi and SW UMa (Connon Smith et al. 1997). In particular, SW UMa resembles CX128 in the strength of its Balmer lines. *Chandra* detected 15 counts during the discovery observation which yield $L_{\rm x}(d, N_{\rm H} = 10^{21}) = 1.2 \times 10^{31} \times (\frac{d}{1.0\,{\rm kpc}})^2$ erg s^{-1}. If the source is at a distance of ∼1 kpc, the X-ray luminosity is consistent with the luminosities found in quiescent dwarf novae (Byckling et al. 2010).

CX137 = CXOGBS J175553.2−281633, a low accretion rate CV or qLMXB?

Based on the positional coincidence with the X-ray source, Udalski et al. (2012) identified in their OGLE-IV data the optical counterpart to CX137: a 0.431 04 d periodic variable with $I = 15.11$, $V - I = 1.32$. They suggest that the light curve morphology is consistent with an eclipsing binary harbouring a spotted star.

The VIMOS spectrum of the counterpart is dominated by photospheric absorption features (see Fig. 2). Clearly detected is the discontinuity in the continuum at λ5200 caused by the Mg *b* triplet and molecular MgH. Also visible are the metallic blends at λλ6165, 6495. In the red, the Na I doublet and Ca II triplet are found in absorption. Finally, TiO bands are not detected in the spectral range covered by the spectrum. These spectroscopic characteristics are consistent with those expected from a late G-type/early K-type star (see e.g. Jacoby, Hunter & Christian 1984). However, the EW of the Ca II λ8542 line is $\lesssim$2 Å, lower than the $\gtrsim$ 3 Å observed in stars with the above spectral types (see for instance fig 23 in Carquillat et al. 1997). Note that the line measurements are not affected of contamination from a partially resolved field star located SE from CX137. The low EWs may indicate an additional source of continuum light veiling the photospheric lines, for instance the accretion disc. On the other hand, the discrepancy in the EWs is not likely to be due to Paschen emission as there is no evidence of other hydrogen emission lines in the red part of the spectrum. The presence of broad Hα in emission also supports an accreting binary nature for CX137. From single Gaussian fitting, we conclude that the Hα profile has an intrinsic FWHM and EW larger than 960 km s^{-1} and 6.5 Å, respectively. While the line position is consistent with its rest wavelength, we measure a -90 ± 20 km s^{-1} RV for the NaD and Ca II photospheric lines found in the red part of the spectrum.

The optical counterpart to CX137 is the brightest in the sample of GBS sources discussed in this paper and it is saturated in most of the Mosaic-II data. As a result, no meaningful variability information is available from the Mosaic-II images. We therefore investigated the publicly available OGLE-IV data sets which at the time of writing consist on a total of 4358 data points in the *I* band acquired during the years 2010–2012. Visual inspection of the light curves suggested small changes in brightness and/or morphology during the three years, and therefore, we analysed each year separately. We measure a mean *I*-band magnitude of 15.11, 15.08 and 15.10 (with an rms of 0.06 mag) and $\Delta r'$ of 0.20, 0.24 and 0.23 mag for 2010, 2011 and 2012, respectively. Periodograms computed for each year have the highest peak centred at 0.215 517 25(15) d, where the numbers in parentheses quotes the uncertainty in the last digits. This is half of the orbital period since the light curves phase folded on the 0.4 d period show a much less scattered sinusoidal-like modulation than when folded on the 0.2 d periodicity. Thus, we confirm the orbital period found by Udalski et al. (2012). The folded light curves (see Fig. 4) show that during 2010 the two maxima and two minima have similar brightness. In contrast, during 2011 and 2012 both minima and maxima occur at different brightness levels. Another characteristic of the light curve is the lack of strong flickering, which supports a stellar component as the main contributor to the optical light.

Udalski et al. (2012) interpreted the sinusoidal light curve as due to eclipses in a contact binary where the yearly changes are due to star spots. On the other hand, the light curve morphology can be explained as due to ellipsoidal variability of the companion star in an accreting system observed at low or moderate inclination. In this scenario, the long-term variability observed in the ellipsoidal light curve can also be associated with star spots. Other unknown mechanisms may also be at play causing the changes in the light curve morphology (see e.g. Thomas et al. 2012; Ratti et al. 2013a).

In an interactive binary, the mean density of the Roche lobe-filling donor star can be determined from the orbital period by

following Eggleton (1983): $\bar{\rho}(\mathrm{g\,cm^{-3}}) \cong 110 P^{-2}(\mathrm{h}) = 1.0$. This indicates that the donor star in CX137 is enlarged compare to G–K main-sequence stars since the latter have higher mean densities (the 1.4 g cm^{-3} of our Sun, for instance). We adopt a K5 V companion ($M_V = 7.35$, $M_r' = 6.98$, $M_I = 5.73$), null reddening and disc contribution to the optical light to derive a crude lower limit to the distance of 0.7 kpc. Additionally, we use the 15 counts detected with *Chandra* to derive an lower limit on the luminosity of $L_{\rm x}(d, N_{\rm H} = 10^{21}) > 5.8 \times 10^{30} \times (\frac{d}{0.7\,\mathrm{kpc}})^2$ erg s^{-1}.

The detection of photospheric lines and a broad Hα emission line in the optical spectrum suggest that CX137 is a CV accreting at low accretion rate or a qLMXB. High-resolution spectroscopy will show if CX377 is a single (accreting) or double-lined (contact) binary.

CX142 = CXOGBS J174403.7−312305, a CV with an accretion-dominated optical spectrum

The VIMOS spectrum of CX142 (Fig. 2) shows a source rich in narrow emission lines and lacking photospheric absorption features. DIBs are not observed. At blue wavelengths Hα (with intrinsic broadening of 340 ± 20 km s^{-1}) and He I λλ5876, 6678, 7065 lines are visible in emission. In the red, the Ca II triplet at λλ8542, 8662, 8498 are prominent emission lines. They are stronger than the nearest hydrogen lines of the Paschen series – EW(Ca II)/EW(P14) ∼2.

The Mosaic-II light curve (Appendix A) shows an rms scatter of 0.2 mag which is only twice the average statistical error in the photometry. Even though $\Delta r' = 0.6$ mag, the source is at the faint edge of what the Blanco observations can detect, making it difficult to set strong constraints on the optical variability.

The optical counterpart to CX142 shows spectroscopic characteristics similar to those of a CV accreting at high rate or low accretion rate CV with a major contribution from the disc to the total optical light. The low FWHM values found for all the emission lines (Table 2) support a system observed at low inclination if the emission-line region is the accretion disc. Given the good quality of the spectrum, we speculate that CX142 was observed in outburst, well above the $r' = 22.2$ brightness measured in the Mosaic-II photometry. We lack other objects in the slit to confirm this possibility and thereby confirm a dwarf nova CV nature. We infer $L_{\rm x}(d, N_{\rm H} = 10^{21}) = 1.1 \times 10^{31} \times (\frac{d}{1.0\,\mathrm{kpc}})^2$ erg s^{-1} from the 14 counts detected with *Chandra*. Finally, note that strong emission lines from the Ca II infrared triplet have been already reported in CVs. For instance, see the spectrum of the dwarf nova system UU Aql near quiescence (Connon Smith et al. 1997) or GW Lib in outburst (van Spaandonk et al. 2010).

CX154 = CXOGBS J173838.7−283539, a low accretion rate CV or qLMXB

Two epochs of spectroscopy separated by about two weeks were acquired, with the second epoch being of higher quality. This is shown in Fig. 2. Hα in emission is observed in both nights, while He I λ6678 is only detected in the second observation. The Hα emission line is weak (EW ∼ 8 Å) with an unresolved profile. In the red, the Ca II λ8542 appears to be present in absorption with EW ∼ 1.0 Å and an RV of ∼120 km s^{-1} in both nights. This line is most certainly a photospheric feature intrinsic to CX154 and not due to contamination from a nearby field star. Finally, from the Mosaic-II data we derive $\Delta r' = 0.5$ mag and an rms scatter of 0.1 mag.

Based on the likely detection of one of the components of the ionized Calcium triplet, CX154 can be tentatively classified as a low accretion rate CV or qLMXB. The low FWHM shown by Hα could be interpreted as originating in a low-inclination system if the emission arises from an accretion disc. An alternative scenario is that where the line is produced in the donor star by reprocessing of X-rays from a neutron star or white dwarf primary (e.g. Bassa et al. 2009; Ratti et al. 2012; Rodríguez-Gil et al. 2012b). From the 14 counts observed with *Chandra*, we estimate $L_{\rm x}(d, N_{\rm H} = 10^{21}) = 1.1 \times 10^{31} \times (\frac{d}{1.0\,\mathrm{kpc}})^2$ erg s^{-1}.

CX207 = CXOGBS J174625.3−263133, a likely polar

Spectra of the optical counterpart to CX207 were obtained in two nights separated one month. In both nights, the spectrum is dominated by strong Hα in emission (EV > 80 Å). This line is remarkable for being single-peaked despite its broadening (FWHM = 1500–1600 km s^{-1}) and because it presents a large RV offset (|RV| > 350 km s^{-1}) with respect to its rest wavelength. Weaker He I and Paschen emission is also detected in the spectrum. Hα and some of the other features are consistent with having two-component line profiles. The two epochs of spectroscopy show clear variability in the line profiles, in particular their central wavelengths (see Table 2).

The optical light curve for CX207 (Fig. 4) shows an eclipse of a depth more than 3 mag at HJD 245 5389.590 991 and a possible second eclipse in progress at HJD 245 5386.633 003 when the source is observed 1 mag fainter than its mean brightness. Outside these two events, the Mosaic-II data has $\Delta r' = 0.7$ and aperiodic variability with an rms of 0.2 mag.

The optical spectrum of CX207 resembles that of the neutron star X-ray binary Circinus X-1 (Mignani, Caraveo & Bignami 1997; Johnston et al. 2001; Jonker et al. 2007) or the black hole transient V4641 Sagittari (Lindstrøm et al. 2005). In this case, the large broadening, large RV offset and variability may be due in part to an outflow in an active X-ray binary harbouring a compact primary and an early-type companion. This model for CX207 requires the X-ray binary to be at a large distance and suffer significant reddening in order to explain the faintness of the X-ray and optical counterparts (11 *Chandra* counts equivalent to $L_{\rm x}(d, N_{\rm H} = 10^{21}) = 8.7 \times 10^{30} \times (\frac{d}{1.0\,\mathrm{kpc}})^2$ erg s^{-1}, $r' = 21.1$). However, the optical spectrum lacks evidence for strong DIBs ruling out this scenario and favours the possibility that CX207 is a nearby CV. In this regard, broad single-peaked emission lines are typically observed in nova-like variables. In this class of high accretion rate CVs, even eclipsing systems do not show a double-peaked profile. The optical spectra in nova-like CVs can show emission lines that reach profile broadenings of values similar to that observed in CX207 (see e.g. Rodríguez-Gil et al. 2007a,b; Dhillon et al. 1992). In this scenario, the large RV offset observed in CX207 will have to reflect a combination of a large systemic velocity and K_1. Alternatively, CX207 may be a member of the magnetic (polar) class of CVs. These systems can exhibit emission lines with similar line morphology and large EWs as observed in the GBS source. In polars, the line profile is composed of (at least) a narrow and a broad component, the former originating in the irradiated donor star. These components can exhibit radial velocities comparable or larger than those measured here – see for instance the eclipsing polars EXO 033319−2554.2 (Allen et al. 1989), MN Hya (Ramsay & Wheatley 1998) and the non-eclipsing system ET Can (Williams et al. 2013), Given that the observed systemic radial velocities in nova-like CVs do not go above ∼200 km s^{-1} (Ak et al. 2010), the magnetic CV scenario seems more likely as it does not require of

such unusual high γ to explain the radial velocities of the emission lines in CX207.

CX377 = CXOGBS J174316.5−274537, a likely low accretion rate CV or qLMXB

Two epochs of spectroscopy separated by nearly two months were obtained with VIMOS. In Fig. 2, we show the spectrum obtained on 2011 Jul 23 UT with the slit oriented such to avoid spatial blending with the nearby field stars. Hα is unambiguously detected in emission. Unfortunately, instrumental artefacts are also apparent in the blue part of the spectra. This makes it difficult to address the presence/absence of stellar features and interstellar bands at wavelengths shorter than Hα. To achieve the detection of photospheric lines, we extracted and studied the spectra of field stars in the CX377 slit. In this way, we confirm the non-detection of the metallic blends at $\lambda\lambda$6165, 6495 which are strong features in the spectra of late-type stars. We cannot establish the presence of He I emission at λ6678. In the red, the spectrum reveals the absorption lines from the Ca II infrared triplet. On the other hand, neither the Na I double nor the P14 λ8598 line or TiO bands appear to be present at the time of the observations. These spectroscopic characteristics suggest a late F-type/early G-type donor star in CX377 (see e.g. Jacoby et al. 1984; Zhou 1991; Munari & Tomasella 1999). We measure for the Ca II λ8542 line an EW of $\sim$1.5 Å, lower than the values observed in F/G of any luminosity class (Jones, Alloin & Jones 1984; Zhou 1991). As in CX137 this discrepancy can be due to veiling of the lines by the accretion disc continuum emission. Disc veiling could also explain the non-detection of the metallic lines described above.

During the two epochs of spectroscopy the profile of the Hα emission line is intrinsically broadened by $\sim$1200 km s^{-1} (FWHM) and asymmetrically double-peaked with the blue peak being stronger than the red peak. The double-peak separation is $\Delta v = 610 \pm 20$ and 720 ± 30 km s^{-1} during the first and second epoch, respectively. Given the asymmetry in the line profiles, a better estimation of the line centre than that obtained from a Gaussian fit (Table 2) is provided by the centroid of the line derived from the emission-line peaks. We measure in this way radial velocities of 70 ± 20 and 60 ± 30 km s^{-1} for the first and second epoch, respectively. Both values are consistent within the errors. On the other hand, we derive from the Ca II triplet radial velocities of 80 ± 6 and 90 ± 10 km s^{-1} for epoch 1 and 2, respectively. These velocities are consistent with those measured from Hα. Note here that the emission line is weak (EW$\sim$7 Å) and thereby its double-peak morphology may be caused by the underlying photospheric Hα.

The VIMOS spectra also show the λ8620 DIB with an EW = 0.7 $\pm$ 0.1 Å. We derive $E(B-V) = 1.9 \pm 0.2$ according to the relation between reddening and EW for this interstellar band (Munari 2000). This value is equal to the 1.9 ± 0.3 mag derived from the reddening maps of the Galactic bulge (Gonzalez et al. 2012; these maps have a spatial resolution of 2×2 arcmin^2 resolution).

The Mosaic-II light curve of CX377 (Appendix A) shows photometric variability with an rms scatter of 0.05 mag and $\Delta r' = 0.2$ mag. There is no evidence for a periodic modulation.

The detection of the donor star in the VIMOS spectrum, the Hα profile broadening (larger than observed in chromospherically active objects) and the high reddening towards the source suggest that CX377 is a (bulge) low accretion rate CV observed at a moderate inclination or a bulge qLMXB. Using the relationship of Bohlin, Savage & Drake (1978) $N_{\rm H} = 5.8 \times 10^{21} \times E(B-V)$ cm^{-2} and adopting as before an absorbed power-law spectrum with index $\Gamma = 2$, we derive from the detect seven *Chandra* counts an unabsorbed flux of 1.0×10^{-13} erg cm^{-2} s^{-1} (0.5–10 keV) and a luminosity of $L_{\rm x}(d, N_{\rm H} = 1.1 \times 10^{22}) = 7.6 \times 10^{32} \times (\frac{d}{8.0\,{\rm kpc}})^2$ erg s^{-1}.

CX446 = CXOGBS J174627.1−254952, a high inclination CV or qLMXB

The spectrum of the optical counterpart to CX446 can be found in Fig. 3. Due to its low signal-to-noise ratio, we only detect strong Hα in emission with EW = 50 ± 4 Å. The line profile appears single-peaked despite its large intrinsic broadening (FWHM = 2200 ± 50 km s^{-1}). This appearance may be caused both by noise and/or the presence of a narrow emission-line component filling-in the region between the two peaks. The large line broadening is suggestive of a high-inclination system. The Mosaic-II light curve (Appendix A) shows a dimming event at HJD 245 5387.824 233 with a 0.4 mag depth with respect to a mean 21.16 r'-band magnitude. Our photometric sampling does not allow us to set constraints on the duration of this event or whether this and other decreases in brightness are consistent with eclipses or dips rather than photometric variability. We performed a periodicity analysis of this light curve but this yielded no significant period.

In summary, the broadening of the line and the eclipse-like event observed in the light curve suggest a high-inclination (eclipsing) CV or qLMXB nature for CX446. From the six counts detected by *Chandra*, we estimate $L_{\rm x}(d, N_{\rm H} = 10^{21}) = 4.7 \times 10^{30} \times (\frac{d}{1.0\,{\rm kpc}})^2$ erg s^{-1}.

CX522 = CXOGBS J175432.5−282918, a CV with an accretion-dominated optical spectrum

The optical counterpart to this GBS source was misidentified in Udalski et al. (2012) with a close bright field star. The coordinates for the correct optical counterpart to CX522 can be found in Table 1. The VIMOS spectrum (Fig. 3) shows Hβ and He I $\lambda\lambda$5876, 6678, 7065 with some evidence for Paschen emission in the red part of the spectrum. Hα is moderately broad with 850 ± 10 km s^{-1} FWHM. Neither photospheric lines from the donor star nor strong DIBs are detected.

The optical counterpart to CX522 is too close to the bright field star mentioned above to allow for a reliable photometric study on the Mosaic-II data. From the VIMOS pre-images obtained on 2011 Apr 8 UT, we derive $R \sim 22$ by performing differential photometry respect to the USNO B1.0 object 0615-0617155 ($R1 = 18.68$). On the other hand, examination of the spatial profile of both the optical counterpart spectrum and the spectrum of a field star partially contained in the slit suggests that CX522 may have been brighter at the time of the spectroscopic observations.

On the basis of the spectroscopic characteristics described above, CX522 is a high accretion rate CV or a low accretion rate CV with an accretion-dominated optical continuum. The five counts detected with *Chandra* imply $L_{\rm x}(d, N_{\rm H} = 10^{21}) = 4 \times 10^{30} \times (\frac{d}{1.0\,{\rm kpc}})^2$ erg s^{-1}.

CX772 = CXOGBS J174405.0−263159

Only broad Hα in emission with an intrinsic FWHM of 900 ± 180 km s^{-1} is apparent in the VIMOS spectrum (Fig. 3). On the other hand, it is not possible to address the presence of line features in the red part of the spectrum given that the spectrum is affected

by fringing – the observations were taken before the upgrade of the VIMOS detectors (see Section 2.1).

We measure $\Delta r' = 1.5$ and an rms scatter of 0.3 mag for the light curve of CX772 (see Appendix A). However, the brightness of the optical counterpart ($r' = 22.2$) is at the faint end of the range of detected objects in the Mosaic-II data. Thus, the photometry has on average a large uncertainty of 0.18 mag.

With the current data we cannot establish the nature of CX207 further than it is a CV or a qLMXB. The four counts detected with *Chandra* yield $L_{\rm x}(d, N_{\rm H} = 10^{21}) = 3.2 \times 10^{30} \times (\frac{d}{1.0\,{\rm kpc}})^2$ erg s^{-1}.

CX781 = CXOGBS J174311.1−271621, a CV with an accretion-dominated optical spectrum

The VIMOS spectrum of CX781 (Fig. 3) exhibits Hα and He I λ6678 emission with unresolved line profiles. The Hα line profile is weak with EW = 5.0 ± 0.2 Å. Instrumental artefacts are evident in the blue part of the spectrum making difficult to identify stellar features and interstellar bands at wavelengths shorter than Hα. In the red part of the spectrum (right-hand panel) absorption lines from the donor star are not detected, in particular, there is no evidence of the Ca II triplet in absorption. Only H I λ9229 (P11) seems to be present, but in emission.

The Mosaic-II light curve for the optical counterpart to CX781 (Appendix A) exhibits clear variability: the source brightness decreases by 0.25 mag four days after the start of the observations to return slowly to full brightness of $r' = 17.9$ mag approximately four days later. Long-term erratic variability usually observed in accreting binaries can explain this behaviour. There is also variability at shorter time-scales (flickering) of 0.05 mag amplitude. We derive $\Delta r' = 0.28$ mag and rms of 0.09 mag from the whole light curve.

The lack of photospheric features in the VIMOS spectrum, the detection of flickering together with possible erratic long-term photometric variability support both a high accretion rate CV nature or a low accretion rate CV where the accretion flow is the dominant source of optical continuum – a short orbital period IP or dwarf nova in quiescence for instance. The narrow and weak Hα emission line is arising either in the disc of a low-inclination binary or in the irradiated hemisphere of the donor star. We estimate $L_{\rm x}(d, N_{\rm H} = 10^{21}) = 3.2 \times 10^{30} \times (\frac{d}{1.0\,{\rm kpc}})^2$ erg s^{-1}.from the five counts detected with *Chandra*.

CX794 = CXOGBS J174142.3−275829, an eclipsing nova-like

Udalski et al. (2012) reported an $I = 19.4$ optical counterpart to CX794 and found in the OGLE light curve a possible 0.117 86 d period together with evidence for eclipses. Dimming events of up to 2 mag are apparent in the Mosaic-II photometry (Fig. 4) as well as in the public OGLE light curve. A Lomb–Scargle periodogram analysis of our data shows a 0.1179 d period with another peak at 0.1052 d, adding weight to the period reported by Udalski et al. (2012). The long (∼2 yr) interval spanned by the OGLE observations allows us to assess the eclipsing nature of CX794 and establish its orbital period by using an O−C curve analysis. For this, we have taken the minimum brightness in the OGLE light curve to be the event closest to or at the time of a mid-eclipse. This yields the following ephemeris: $T_{\rm mid-eclipse}$ = HJD 245 5768.578 74 + 0.117 86 × E. Next, the times for 11 events with a >0.6 mag drop in brightness were identified in both the OGLE and Mosaic-II data. The O−C curve (not shown) displays <0.1 cycles offsets between these times and the eclipse times derived from the ephemeris. The same analysis shows that the periodicities found in the Mosaic-II data gave larger residuals. Fig. 4 shows the Mosaic-II light curve folded on the above ephemeris.

Our optical spectrum (Fig. 3) shows Hα, Hβ and He I $\lambda\lambda$5876, 6678, 7065 lines in in emission. The FWHM of Hα (1050 km s^{-1}) is on the low side for a high-inclination system. Furthermore, the line profiles of both lines are single peaked. Lines from the Paschen series are also detected in emission with P9 being the strongest. On the other hand, there is no evidence for absorption features from the donor star or the interstellar medium.

These above properties suggest that CX794 is a high accretion rate CV within the 2–3 h period gap and with spectroscopic similarities to the SW Sextantis nova-like variables. We derive $L_{\rm x}(d, N_{\rm H} = 10^{21}) = 3.2 \times 10^{30} \times (\frac{d}{1.0\,{\rm kpc}})^2$ erg s^{-1} from the four *Chandra* counts. At present, we lack an infrared counterpart to obtain a reliable constraint on the distance towards the source by using the method by Knigge (2006).

CX1004 = CXOGBS J174623.5−310550, a low accretion rate eclipsing CV or qLMXB

The most remarkable feature in the spectrum of CX1004 (Fig. 3) is a broad double-peaked Hα emission line with FWHM = 2120 ± 20 km s^{-1} and a peak-to-peak velocity separation of $\Delta v = 1170 \pm 10$ km s^{-1}. This is the single emission line detected in the spectrum. The centroid of the Hα line profile measured using the red and blue peak positions yields an RV of −170 ± 20 km s^{-1}, slightly lower than the value obtained by fitting a single Gaussian to the line profile (Table 2). Absorption bands are prominent in the spectral range 5850−7350 Å and are caused by the TiO α, β, γ and γ' band systems [see e.g. Coelho et al. (2005) for their identification in a broad-band spectrum]. Redward of 8000 Å, the δ and ϵ systems are not detected. In this region, the Na I doublet at $\lambda\lambda$8183, 8195 is in absorption together with the Ca II and hydrogen atomic lines. No interstellar features are found, except perhaps for the NaD doublet at $\lambda\lambda$5890, 5896 unresolved from their stellar counterparts. We measure an RV of −170 ± 20 km s^{-1} from fits to the metallic lines in the red part of the spectrum. This value is in agreement with the RV obtained from the Hα emission line.

On the other hand, the Mosaic-II light curve (Appendix A) does not exhibit significant photometric variability for this source in 35 observations. The rms scatter and $\Delta r'$ in the photometry is 0.04 mag and 0.17 mag, respectively.

The large FWHM and peak-to-peak velocity separation in the Hα profile in CX1004 is similar to that observed in eclipsing dwarf novae CVs in quiescence or qLMXBs harbouring a black hole. Examples are OY Car ($P_{\rm orb} = 1.51$ h, $\Delta v = 1160$ km s^{-1}; Schoembs & Hartmann 1983), U Gem ($P_{\rm orb} = 4.22$ h, $\Delta v = 920$ km s^{-1}; Naylor, Allan & Long 2005; Echevarría, de la Fuente & Costero 2007), XTE J1118+480 ($P_{\rm orb} = 4.08$ h, $\Delta v = 1800$ km s^{-1}; Torres et al. 2004) and A0620-00 ($P_{\rm orb} = 7.68$ h, $\Delta v = 1270$ km s^{-1}; Marsh, Robinson & Wood 1994).

As shown above, the detection of photospheric lines and the large broadening of the Hα emission line are properties that suggest that CX1004 is an eclipsing CV accreting at low accretion rate or a high-inclination qLMXB with a black hole primary. However, the lack of significant photometric variability is difficult to explain as we would expect to see eclipses, an ellipsoidal modulation and/or flickering. Finally, the lack of DIBs suggests a nearby source for which we derive from the three *Chandra* counts an X-ray luminosity

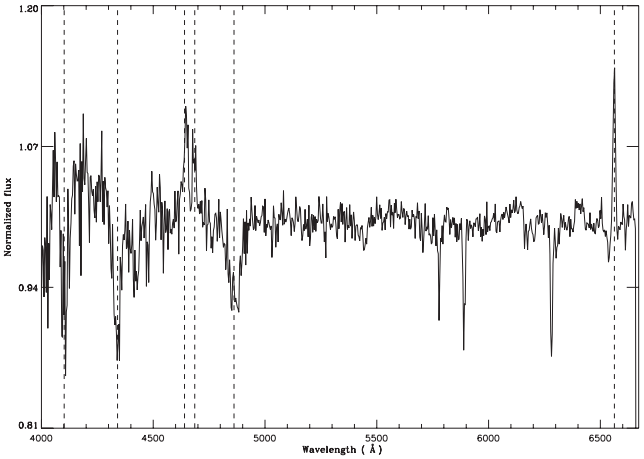

Figure 5. Normalized IMACS spectrum of CX1011. Markers are for Hδ, Hγ, the Bowen blend, He II λ4686, Hβ and Hα. The three prominent absorption features in the region $\lambda\lambda$5800−6300 are interstellar in origin.

of $L_{\rm x}(d, N_{\rm H} = 10^{21}) = 2.4 \times 10^{30} \times (\frac{d}{1.0\,{\rm kpc}})^2$ erg s^{-1}. As a reference an M2 V ($M_r' = 9.14$) unreddened star with the same apparent magnitude as CX1004 will be at a 2.1 kpc distance.

CX1011 = CXOGBS J174604.7−311722, a nova-like variable

A strong feature in the VIMOS and IMACS spectrum (Figs 3 and 5) is Hα with a narrow and weak emission-line profile contained within a broad absorption component. Redward of Hα, He I λ6678 is in emission as well as several Paschen lines with P9 being the strongest of them. In addition to the saturated interstellar NaD doublet, DIBs at λ5780 and λ6284 are prominent with EWs of 0.40 ± 0.03 and 1.28 ± 0.05 Å, respectively. Photospheric lines from the donor star are not detected, in particular, there is no evidence of the Ca II triplet in absorption or emission.

The spectral resolution and blue coverage provided by the IMACS observation (Fig. 5) allows us to measure an intrinsic FWHM of 578 ± 2 km s^{-1} for Hα and we find that the other Balmer lines are composed by a broad absorption component filled-in with core emission. We have measured the full-width zero intensity of the absorption components to be 7522 ± 555, 4964 ± 898 and 4593 ± 950 km s^{-1} for Hβ, Hγ and Hδ, respectively. The large uncertainties are due to the difficulty of defining the continuum. Broad He II λ4686 and the C III/N III Bowen blend near λ4648 are obvious in the IMACS spectrum. We also detect He I λ4471 with emission and absorption components as observed for the Balmer lines.

This source is near the saturation limit of the Mosaic-II data. There are 17 observations which do not saturate. The photometry is characterized by low-amplitude flickering with an rms of 0.03 mag and $\Delta r' = 0.1$. This variability is not significantly correlated with the seeing, which suggests it is real and not a product of the non-linear CCD response at high count rates.

We derive an $E(B - V) = 0.8$ mag from the calibration between reddening and the EW for the λ5780 DIB (Herbig 1993). This value is smaller than the 1.6 ± 0.2 mag obtained from the reddening maps of the Galactic bulge (Gonzalez et al. 2012). Using $N_{\rm H} = 5.8 \times 10^{21} \times E(B - V)$ cm^{-2} (Bohlin et al. 1978) and an absorbed power-law spectrum with photon index $\Gamma = 2$, we calculate from the detected three *Chandra* counts an unabsorbed flux of 5.7×10^{-14} erg cm^{-2} s^{-1} (0.5–10 keV) and X-ray luminosity of $L_{\rm x}(d, N_{\rm H} = 4.6 \times 10^{21}) = 6.1 \times 10^{31} \times (\frac{d}{3.0\,{\rm kpc}})^2$ erg s^{-1}.

The presence of high-excitation emission lines and broad absorption lines of H I and He I partially filled-in by emission cores is frequently observed in nova-like variables (non-magnetic CVs in a state of high accretion rate). The narrow emission cores observed in CX1011 suggests a low-inclination system. However, we cannot exclude an origin for the emission in the irradiated donor star or hotspot instead of the disc as observed in the nova-like IX Vel (Beuermann & Thomas 1990). The optical spectrum of CX1011 resembles that of IX Vel except that in our spectrum we do not detect He I λ4922 in emission and the Bowen blend appears stronger than the He II λ4686 line.

Summary

Table 3 summarizes the optical and X-ray properties discussed in this section. Among the 23 systems, at least 12 of them are CVs with an accretion-dominated optical spectrum (CX28, CX39, CX45, CX63, CX70, CX128, CX142, CX207, CX522, CX781, CX794 CX1011). CX28 is a high accretion rate CV (Britt et al. 2013) while CX39 is most likely a short orbital period dwarf nova. We establish that CX207 is an eclipsing magnetic CV. CX794 and CX1011 are nova-like CVs with the former being eclipsing and in the period gap. The accretion-dominated optical spectrum of the remaining sources is consistent either with CVs in a state of high mass transfer or low accretion rate CVs with the optical spectrum dominated by emission from the accreting disc as observed in short orbital period dwarf novae. Another 6 of the 23 GBS sources (CX44, CX93, CX137, CX154, CX377 and CX1004) show photospheric lines from the donor star in addition to emission lines indicating that they are probably accreting binaries in quiescence or in a low accretion rate state. CX93 is a confirmed low accretion rate CV (Ratti et al. 2013a), while the remaining sources require a dynamical study to establish if they are CVs or qLMXBs. Note here that the large broadening (2100 km s^{-1} FWHM) of the double-peaked Hα emission line in CX1004 suggests that it is a high-inclination or even eclipsing system. Finally, for 5 of the 23 sources (CX64, CX73, CX87, CX446 and CX772) it is unclear whether absorption lines from the donor star are present due to the noise and/or instrumental artefacts in the spectra. However, we find from the optical light curve that CX87 is an outbursting CV. From the VIMOS spectroscopy, the 2100 km s^{-1} FWHM of the Hα emission line in CX446 supports a high inclination for this source.

6 CONCLUSIONS AND REMARKS

In this paper and in Britt et al. (2013), we have utilized optical spectroscopy to identify the emission-line optical counterparts to 27 GBS sources and to classify them as accreting binaries. To derive sample of accreting binaries from the optical counterparts to GBS sources as clean as possible of unrelated objects, we have adopted three discriminators, viz. Hα in emission with (i) EW > 18 Å, (ii) FWHM > 400 km s^{-1} and/or the presence of He I $\lambda\lambda$5876, 6678 emission with EW > 3 Å and EW(He I)/EW(Hα) >0.2. Such a selection towards strong Hα emitters permits us to derive a sample weakly or not contaminated by chromospherically active stars/binaries which are expected to represent ∼40 per cent of the X-ray sources found in the GBS area (Jonker et al. 2011). In fact we have identified with VIMOS a large number of optical counterparts to GBS sources that show spectra characteristic of this type of sources. A disadvantage of using this approach is that accreting binaries with an emission-line spectrum not fulfilling any of the above criteria will be missed. Furthermore, a selection based

only on the detection of objects with emission lines, blue colours or/and a composed disc – donor spectra will neglect sources in quiescence with spectra fully or mostly dominated by the donor star. For instance, the black hole LMXBs 4U 1543−47, GRO J1655−40 and SAX J1819.3−2525 (see Table 4) would have been overlooked since during quiescence the emission lines may become apparent as residual features only after subtracting the donor star spectrum. The same selection caveat can affect systems harbouring less massive primaries. This is the case of IGR J19308+053 (Ratti et al. 2013b) where light from the F-type companion dominates over both

Table 3. Optical and X-ray properties of identified accreting binaries.

No.	GBS ID	Photometry r',rms,$\Delta r'$/ type of variability[a]	Spectroscopy characteristics[b] (accretion,donor)	X-ray (0.5–10 keV) HR[c]	f_x[d]	L_x[e]	Nature and remarks[f]
1	CX28	16.9, 0.2, 0.8/F	AD,H	0.50 ± 0.195	3.0	3.6	H CV
2	CX39	20.2, 0.1, 0.3/O,F	AD	-0.35 ± 0.25	2.4	2.8	AD CV
3	CX44	18.68, 0.05, 0.2/F	L,K-type	-0.19 ± 0.19	2.1	10	NS qLMXB, CV = AX J1755.7-2818
4	CX45	20.4, 0.4, 1.5/F	AD	0.66 ± 0.24	2.1	2.5	AD CV
5	CX63	21.3, 0.2, 0.8/F	AD	0.16 ± 0.23	1.7	2.1	AD CV
6	CX64	22.3,<0.14,–/–	–	0.22 ± 0.23	1.6	2.0	Low state CV, bulge H CV
7	CX70	20.42, 0.08, 0.3/F	AD	0.63 ± 0.29	1.6	1.9	AD CV
8	CX73	18.62, 0.08, 0.3/F	–	0.22 ± 0.25	1.5	1.8	Unknown nature
9	CX87	23.3,–,–/O	–	0.31 ± 0.25	2.8	31	CV
10	CX93[g]	17.25, 0.03, 0.1/ell	L/K5 V		1.2−1.7	0.6−0.9	L CV, = CX153
11	CX128	20.9, 0.2, 0.9/F	AD		1	1.2	AD CV, dwarf nova?
12	CX137[g]	15.1, 0.06, 0.2/ell,EC?	L,G/K-type		1	>0.6	CV, qLMXB?
13	CX142	22.3, 0.2, 0.6/F?	AD		0.9	1.1	AD CV
14	CX154	21.4, 0.1, 0.5/F?	L/–		0.9	1.1	L CV, qLMXB?
15	CX207	21.1, 0.2, 0.7/E,F	AD,H		0.7	0.8	Magnetic (Polar) CV
16	CX377	18.86, 0.05, 0.2/F?	L,F/G-type		1.0	76	L CV, qLMXB
17	CX446	21.2, 0.2, 0.9/dip,E?	–		0.4	0.5	High *i* CV, qLMXB
18	CX522	∼22,–,– /–	AD		0.3	0.4	AD CV
19	CX772	22.2, 0.3, 1.5/F?	–		0.3	0.3	Unknown nature
20	CX781	17.89, 0.09, 0.3/LT,F	AD		0.3	0.3	AD CV
21	CX794[g]	19.9, 0.2, 0.9/F,E(2 mag)	AD,H		0.3	0.3	Nova-like CV
22	CX1004	20.76, 0.04, 0.2/F	L,M-type		0.2	0.2	High *i* CV, qLMXB
23	CX1011	16.18, 0.03, 0.1/–	AD,H		0.6	6.1	Nova-like CV

[a]Mean, rms and maximum variability in the r' band, except for CX87 and CX137 where the values are for the *R* and *I* band, respectively. For eclipsing and outbursting sources quantities are determined excluding such events. Photometric variability types are: E = eclipsing, EC = eclipsing contact binary, ell = ellipsoidal, F = flickering, LT = long-term variability, O = outburst.
[b]AD = accretion-dominated optical spectrum, H,L = High, Low accretion rate.
[c]Hardness ratio (HR) as provided in Jonker et al. (2011). See also Section 5 for the definition of HR.
[d]Unabsorbed f_x in units of 10^{-13} erg cm^{-2} s^{-1} calculated with an absorbed power-law model with $\Gamma = 2$ and $N_{\rm H} = 10^{21}$ cm^{-2} except for CX87 (10^{22} cm^{-2} assumed) and CX93, CX377 and CX1011, where $N_{\rm H}$ is derived from the reddening as $5.8 \times 10^{21} \times E(B-V)$ cm^{-2}. $E(B-V) = 0.6 \pm 0.2$, 1.9 ± 0.2 and 0.8 for CX93, CX377 and CX1011, respectively.
[e]Unabsorbed L_x in units of 10^{31} erg s^{-1}. A 1 kpc distance is assumed except for CX44, CX87, CX93, CX137, CX377 and CX1011, where a distance of 2, 3, 0.66, >0.7, 8 and 3 kpc is used, respectively.
[f]Acronyms are as given in column 4 and in the text.
[g]The orbital periods of CX93, CX137 and CX794 are 0.237, 0.431 and 0.117 86 d, respectively. The orbital parameters of CX93 can be found in the dynamical study of Ratti et al. (2013a).

Table 4. For the sake of completeness and comparison, we provide orbital parameters for several sources examined in Section 6. The abbreviations in the table are as follows: BH = black hole; NS = neutron star; q = mass ratio.

Source	Nature	$P_{\rm orb}$ (day)	γ (km s^{-1})	K_2 (km s^{-1})	q	Companion	Ref.
4U 1543−47	BH LMXB	1.12	−82	124		A2 V	1
GRO J1655−40	BH LMXB	2.62	−142	228	0.33	F3-6 IV	2
SAX J1819.3−2525	BH LMXB	2.82	107	211	0.67	B-TYPE	3
FIRST J102347.6+0038	NS LMXB	0.198	1	268		Mid-G V	4
Centaurus X-4	NS LMXB	0.629	184	150	0.17	K3-5 V	5
Cygnus X-2	NS LMXB	9.84	−210	86	0.34	A9 III	6
IGR J19308+053	CV	0.61	−18	91	1.78	F-type	7

References: (1) Orosz et al. (1998), (2) Orosz & Bailyn (1997), Shahbaz et al. (1999), (3) Orosz et al. (1998), (4) Thorstensen & Armstrong (2005), Wang et al. (2009), (5) Torres et al. (2002), González Hernández et al. (2005), (6) Casares, Charles & Kuulkers (1998), Kolb et al. (2000), (7) Ratti et al. (2013b).

accretion disc and white dwarf emission. Another interesting example is the millisecond radio pulsar FIRST J102347.6+003841 (see also Table 4) where occasionally only photospheric features from the G-type dwarf donor are detected during quiescence. While low in number, such objects are of interest for two reasons: first, A and F donors are visible at larger distances and reddening than cooler companions. Secondly, their optical and infrared counterparts are partially or totally free of variable emission from the accretion disc. As a consequence inclination and distance measurements become less dependent on uncertainties in the disc contribution to the total light. The selection effect also applies to LMXBs in hierarchical triple systems in which the main source of optical light during quiescence is the star orbiting around the inner LMXB. Considering only the two confirmed triple systems among the current sample of recycled millisecond pulsars, we expect an ∼10 per cent of the LMXBs to be triple system.

In order to increase the chances of finding accreting binaries in sources with no or only weak signs of on-going accretion in their optical spectra, spectroscopic surveys should also employ RV measurements. Stellar-like objects with high radial velocities (or proper motions) should be re-observed to confirm if they are binaries. The reason for this is that, except for runaway stars, field stars in the direction of the bulge should show only small radial motions with respect to the Sun. An RV search for accreting binaries will be sensitive to LMXBs with cool (G to M-type) donors and black hole LMXBs with cool (G to M) and hot (A to F-type) donors since in these cases $q \lesssim 1$ and thereby $K_2 \gtrsim 100\,\mathrm{km\,s^{-1}}$ for orbital periods less than a day. Detection of neutron star LMXBs and CVs with hot donors in a single RV measurement is more unlikely since $q \gtrsim 1$ and $K_2 \lesssim 100\,\mathrm{km\,s^{-1}}$ (however, see Ratti et al. 2013b). Furthermore, some neutron star LMXBs may have received a significant natal kick that may result in a high systemic RV for the system. Examples of systems with a high γ are Cyg X-2 and Cen X-4 (see Table 4). Accreting binaries in the bulge may also have a high RV component caused by the kinematics in this region. Bulge members can be identified by the presence of strong DIBs in their optical spectra. The strengths in many of these features correlate well with the extinction towards the source and thereby they can be used together with 2D/3D extinctions maps of the GBS areas (e.g. Gonzalez et al. 2012; Chen et al. 2013). The GBS, with a selection of sources based on their X-ray detection, a spectroscopic search accounting for radial velocities and a photometric scrutiny to identify ellipsoidal variables, will allow us to investigate the frequency and nature of accreting binaries lacking signs for accretion activity in their optical spectra.

To distinguish qLMXBs from CVs is non-trivial and it turns out that the only secure identification relies on RV studies (cf. Ratti et al. 2013a). Emission-line properties and/or photometric variability can single out some sub-classes. For instance, cases where CVs show optical outbursts lacking bright X-ray counterparts (e.g. CX39 and CX87). Finally, this paper focuses on the spectroscopic properties of optical counterparts to GBS sources. However, a fraction of the X-ray sources under study is found in heavily reddened regions and can be best studied using their infrared counterparts. Therefore, infrared spectroscopy will have to be obtained in order to classify those sources (see e.g. Greiss et al. 2014).

ACKNOWLEDGEMENTS

We are thankful to Marina Rejkuba (ESO) for supporting our service mode observations with VIMOS. We are grateful to Eva Ratti, Oliwia Madej and Marianne Heida and for helping in the preparation of the VIMOS masks. We also thank Victoria Gabb and Monique Villar for assistance with Mosaic-II data analysis and Lauren Gossen for assistance at the Blanco telescope. PGJ acknowledges support from a VIDI grant from the Netherlands Organization for Scientific Research. DS acknowledges support from STFC through an Advanced Fellowship (PP/D005914/1) as well as grant ST/I001719/1 RIH, CTB and CBJ acknowledge support from the National Science Foundation under Grant no. AST-0908789. This research has made use of the SIMBAD database, operated at CDS, Strasbourg, France.

REFERENCES

Ak T., Bilir S., Ak S., Coşkunoğlu K. B., Eker Z., 2010, New Astron., 15, 491
Alard C., 2000, A&AS, 144, 363
Alard C., Lupton R. H., 1998, ApJ, 503, 325
Allen R. G., Berriman G., Smith P. S., Schmidt G. D., 1989, ApJ, 347, 426
Armas Padilla M., Degenaar N., Wijnands R., 2013, MNRAS, 434, 1586
Barrado y Navascués D., Martín E. L., 2003, AJ, 126, 2997
Baskill D. S., Wheatley P. J., Osborne J. P., 2005, MNRAS, 357, 626
Bassa C. G., Jonker P. G., Steeghs D., Torres M. A. P., 2009, MNRAS, 399, 2055
Beuermann K., Thomas H.-C., 1990, A&A, 230, 326
Bigelow B. C., Dressler A. M., 2003, Proc. SPIE, 4841, 1727
Bilir S., Karaali S., Tunçel S., 2005, Astron. Nachr., 326, 321
Bleach J. N., Wood J. H., Smalley B., Catalán M. S., 2002, MNRAS, 335, 593
Bohlin R. C., Savage B. D., Drake J. F., 1978, ApJ, 224, 132
Bottini D. et al., 2005, PASP, 117, 996
Britt C. T. et al., 2013, ApJ, 769, 120
Byckling K., Mukai K., Thorstensen J. R., Osborne J. P., 2010, MNRAS, 408, 2298
Carquillat M. J., Jaschek C., Jaschek M., Ginestet N., 1997, A&AS, 123, 5
Casares J., Charles P. A., Kuulkers E., 1998, ApJ, 493, L39
Chen B. Q., Schultheis M., Jiang B. W., Gonzalez O. A., Robin A. C., Rejkuba M., Minniti D., 2013, A&A, 550, A42
Coelho P., Barbuy B., Meléndez J., Schiavon R. P., Castilho B. V., 2005, A&A, 443, 735
Connon Smith R., Sarna M. J., Catalan M. S., Jones D. H. P., 1997, MNRAS, 287, 271
Covey K. R. et al., 2008, ApJS, 178, 339
Cox A. N., 2000, Allen's Astrophysical Quantities. AIP Press, New York
Dhillon V. S., 1996, in Evans A., Wood J. H., eds, IAU Colloq. 158: Cataclysmic Variables and Related Objects. Kluwer, Dordrecht, p. 3
Dhillon V. S., Jones D. H. P., Marsh T. R., Smith R. C., 1992, MNRAS, 258, 225
Echevarría J., de la Fuente E., Costero R., 2007, AJ, 134, 262
Eggleton P. P., 1983, ApJ, 268, 368
Foulkes S. B., Haswell C. A., Murray J. R., Rolfe D. J., 2004, MNRAS, 349, 1179
González Hernández J. I., Rebolo R., Peñarrubia J., Casares J., Israelian G., 2005, A&A, 435, 1185
Gonzalez O. A., Rejkuba M., Zoccali M., Valenti E., Minniti D., Schultheis M., Tobar R., Chen B., 2012, A&A, 543, A13
Greiss S., Steeghs D., Maccarone T., Jonker P. G., Torres M. A. P., Gonzalez O., Masetti N., Rojas A., 2011a, Astron. Telegram, 3562, 1
Greiss S. et al., 2011b, Astron. Telegram, 3688, 1
Greiss S. et al., 2014, MNRAS, 438, 2839
Hamann F., Persson S. E., 1992, ApJS, 82, 247
Herbig G. H., 1993, ApJ, 407, 142
Hynes R. I. et al., 2012a, ApJ, 761, 162
Hynes R. I., Britt C. T., Jonker P. G., Wijnands R., Greiss S., 2012b, Astron. Telegram, 4417, 1
Hynes R. I. et al., 2014, ApJ, 780, 11
Ishioka R. et al., 2002, PASJ, 54, 581
Izzo C., Kornweibel N., McKay D., Palsa R., Peron M., Taylor M., 2004, The Messenger, 117, 33

Jacoby G. H., Hunter D. A., Christian C. A., 1984, ApJS, 56, 257
Jester S. et al., 2005, AJ, 130, 873
Johnston H. M., Wu K., Fender R., Cullen J. G., 2001, MNRAS, 328, 1193
Jones J. E., Alloin D. M., Jones B. J. T., 1984, ApJ, 283, 457
Jonker P. G., Nelemans G., Bassa C. G., 2007, MNRAS, 374, 999
Jonker P. G. et al., 2011, ApJS, 194, 18
Jonker P. G., Miller-Jones J. C. A., Homan J., Tomsick J., Fender R. P., Kaaret P., Markoff S., Gallo E., 2012, MNRAS, 423, 3308
Jonker P. G. et al., 2014, ApJS, 210, 18
Kafka S., Honeycutt R. K., Howell S. B., Harrison T. E., 2005, AJ, 130, 2852
Knigge C., 2006, MNRAS, 373, 484
Kolb U., Davies M. B., King A., Ritter H., 2000, MNRAS, 317, 438
Le Fèvre O. et al., 2003, Proc. SPIE, 4841, 1670
Lindstrøm C., Griffin J., Kiss L. L., Uemura M., Derekas A., Mészáros Sz., Székely P., 2005, MNRAS, 363, 882
Maccarone T. J. et al., 2012a, MNRAS, 426, 3057
Maccarone T. J. et al., 2012b, Astron. Telegram, 4109, 1
Marsh T. R., Robinson E. L., Wood J. H., 1994, MNRAS, 266, 137
Mignani R., Caraveo P. A., Bignami G. F., 1997, A&A, 323, 797
Mohanty S., Basri G., 2003, ApJ, 583, 451
Munari U., 2000, in Porceddu I., Aiello S., eds, Proc. Italian Physical Society, Vol. 67, Molecules in Space and in the Laboratory. Italian Physical Society, Bologna, p. 179
Munari U., Tomasella L., 1999, A&AS, 137, 521
Naylor T., Allan A., Long K. S., 2005, MNRAS, 361, 1091
Nelemans G., Jonker P. G., Marsh T. R., van der Klis M., 2004, MNRAS, 348, L7
Nelemans G., Jonker P. G., Steeghs D., 2006, MNRAS, 370, 255
Orosz J. A., Bailyn C. D., 1997, ApJ, 477, 876
Orosz J. A., Jain R. K., Bailyn C. D., McClintock J. E., Remillard R. A., 1998, ApJ, 499, 375
Osterbrock D. E., Fulbright J. P., Martel A. R., Keane M. J., Trager S. C., Basri G., 1996, PASP, 108, 277
Osterbrock D. E., Fulbright J. P., Bida T. A., 1997, PASP, 109, 614
Özel F., Psaltis D., Narayan R., McClintock J. E., 2010, ApJ, 725, 1918
Ramsay G., Wheatley P. J., 1998, MNRAS, 301, 95
Ratti E. M., Steeghs D. T. H., Jonker P. G., Torres M. A. P., Bassa C. G., Verbunt F., 2012, MNRAS, 420, 75
Ratti E. M. et al., 2013a, MNRAS, 428, 3543
Ratti E. M. et al., 2013b, MNRAS, 431, L10
Reipurth B., Pedrosa A., Lago M. T. V. T., 1996, A&AS, 120, 229
Reis R. C., Wheatley P. J., Gänsicke B. T., Osborne J. P., 2013, MNRAS, 430, 1994
Rodríguez-Gil P., Schmidtobreick L., Gänsicke B. T., 2007a, MNRAS, 374, 1359
Rodríguez-Gil P. et al., 2007b, MNRAS, 377, 1747
Rodríguez-Gil P., Schmidtobreick L., Long K. S., Shahbaz T., Gänsicke B. T., Torres M. A. P., 2012a, Mem. Soc. Astron. Ital., 83, 602
Rodríguez-Gil P., Schmidtobreick L., Long K. S., Gänsicke B. T., Torres M. A. P., Rubio-Díez M. M., Santander-García M., 2012b, MNRAS, 422, 2332
Rojas A. F., Greiss S., Masetti N., Steeghs D., Minniti D., 2012, Astron. Telegram, 4006, 1
Sakano M., Koyama K., Murakami H., Maeda Y., Yamauchi S., 2002, ApJS, 138, 19
Schoembs R., Hartmann K., 1983, A&A, 128, 37
Shahbaz T., van der Hooft F., Casares J., Charles P. A., van Paradijs J., 1999, MNRAS, 306, 89
Shaw R. A., ed., 2009, NOAO Data Handbook (Version 1.1). National Optical Astronomical Observatory, Tucson
Shears J., Boyd D., Poyner G., 2006, J. Br. Astron. Assoc., 116, 244
Telleschi A., Güdel M., Briggs K. R., Audard M., Palla F., 2007, A&A, 468, 425
Thomas H.-C., Beuermann K., Reinsch K., Schwope A. D., Burwitz V., 2012, A&A, 546, A104
Thorstensen J. R., Armstrong E., 2005, AJ, 130, 759
Torres M. A. P., Casares J., Martínez-Pais I. G., Charles P. A., 2002, MNRAS, 334, 233
Torres M. A. P., Callanan P. J., Garcia M. R., Zhao P., Laycock S., Kong A. K. H., 2004, ApJ, 612, 1026
Torres M. A. P., Garcia M. R., Steeghs D., McClintock J. E., 2005, ApJ, 632, 514
Udalski A. et al., 2012, Acta Astron., 62, 133
van Paradijs J., Augusteijn T., Stehle R., 1996, A&A, 312, 93
van Spaandonk L., Steeghs D., Marsh T. R., Torres M. A. P., 2010, MNRAS, 401, 1857
Walter F. M., Basri G. S., 1982, ApJ, 260, 735
Wang Z., Archibald A. M., Thorstensen J. R., Kaspi V. M., Lorimer D. R., Stairs I., Ransom S. M., 2009, ApJ, 703, 2017
Warner B., 1995, Cambridge Astrophysics Series Vol. 28, Cataclysmic Variable Stars. Cambridge Univ. Press, Cambridge
Werner K., Nagel T., Rauch T., Hammer N. J., Dreizler S., 2006, A&A, 450, 725
Williams K. A., Howell S. B., Liebert J., Smith P. S., Bellini A., Rubin K. H. R., Bolte M., 2013, AJ, 145, 129
Zacharias N. et al., 2010, AJ, 139, 2184
Zhou X., 1991, A&A, 248, 367

APPENDIX A: OPTICAL LIGHT CURVES

In this appendix, we provide the Mosaic-II light curves of 14 GBS sources that do not show clear periodic or long-term photometric modulation. Note that the light curves for CX28 and CX93 can be found in Britt et al. (2013) and Ratti et al. (2013a). No suitable data were available to obtain a light curve for CX522.

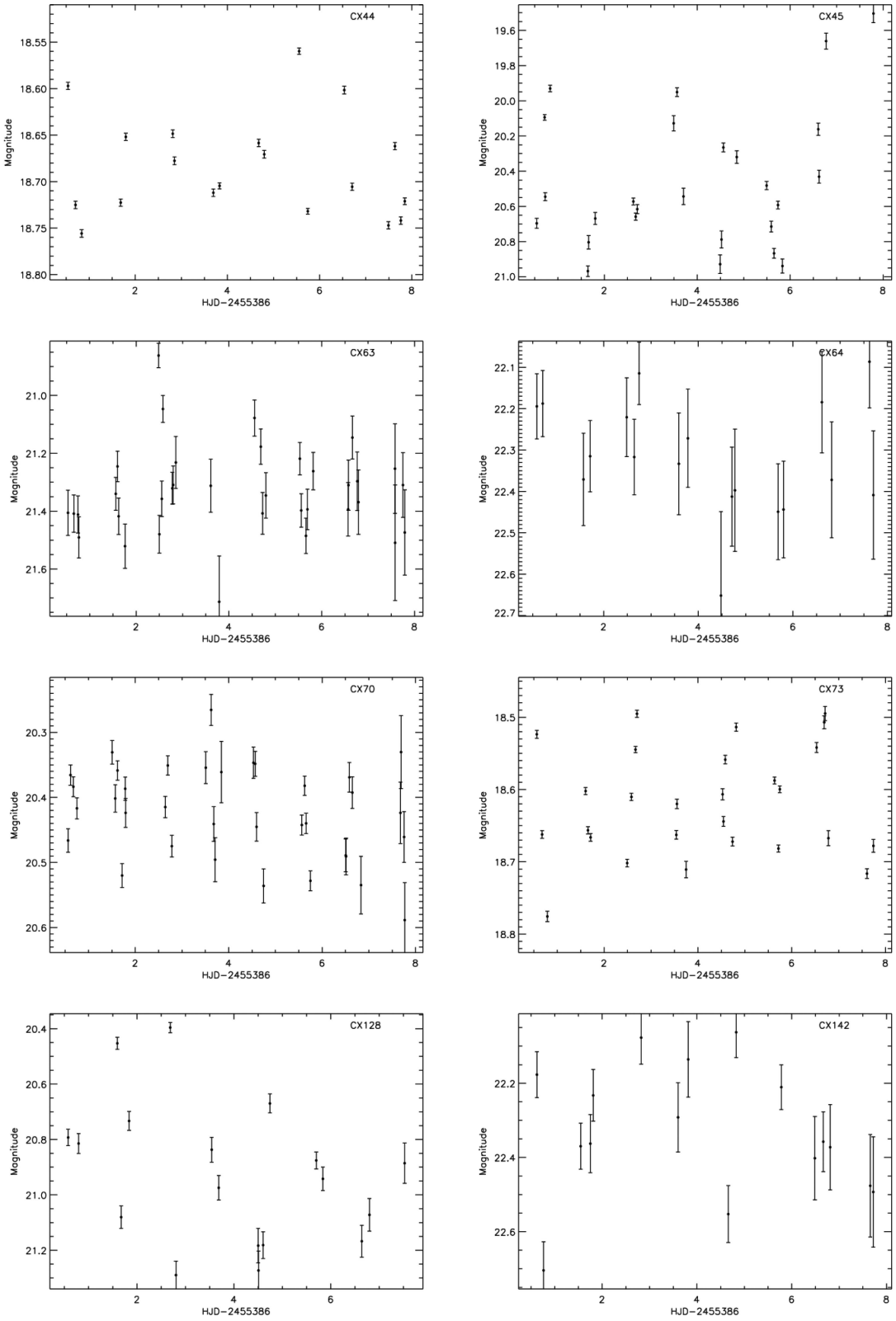

Figure A1. Optical light curves.

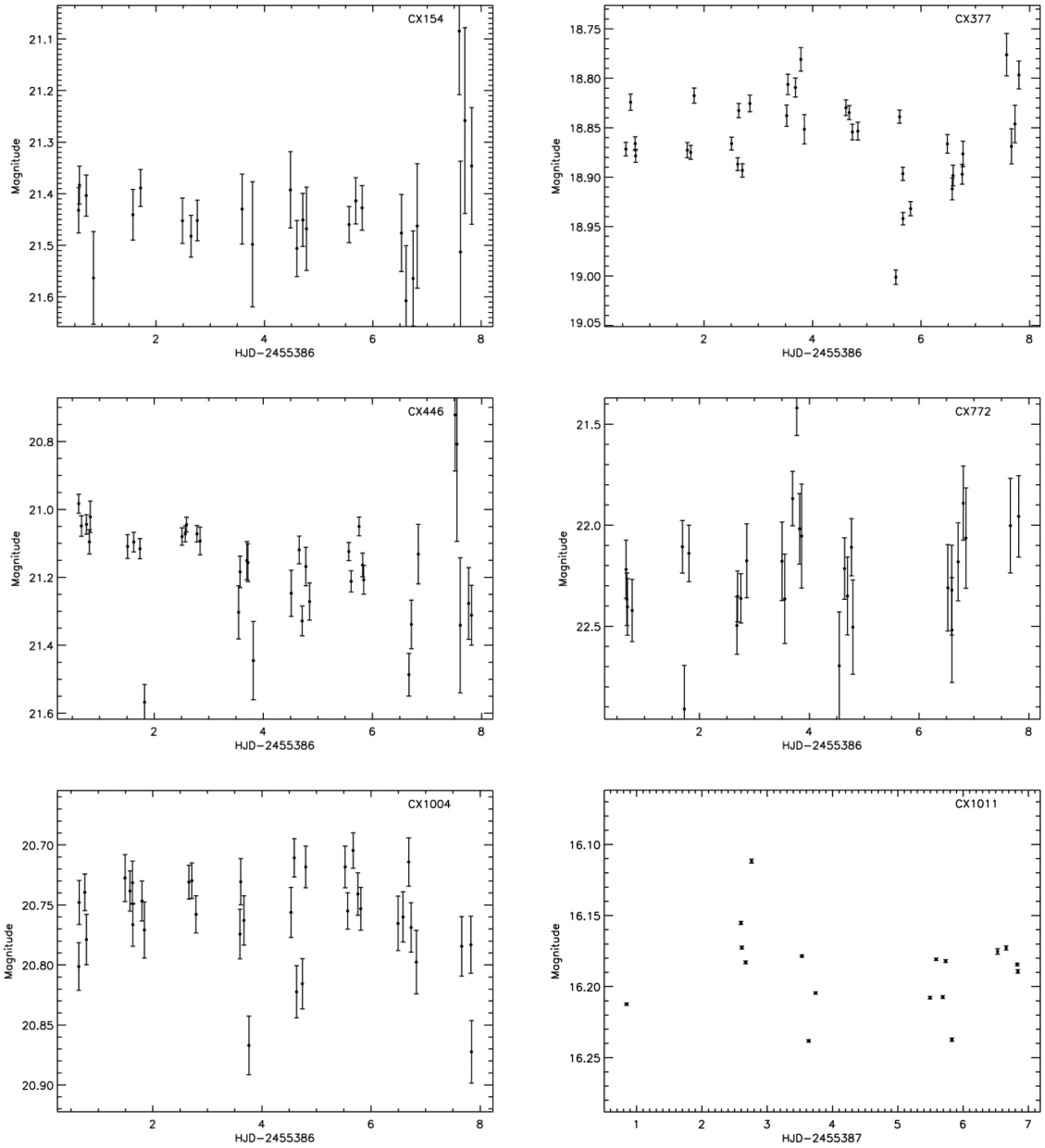

Figure A2. Optical light curves (continued from Fig. A1).

SUPPORTING INFORMATION

Additional Supporting Information may be found in the online version of this article:

Appendix B. Finding charts (http://mnras.oxfordjournals.org/lookup/suppl/doi:10.1093/mnras/stu170/-/DC1).

Please note: Oxford University Press are not responsible for the content or functionality of any supporting materials supplied by the authors. Any queries (other than missing material) should be directed to the corresponding author for the article.

This paper has been typeset from a TEX/LATEX file prepared by the author.